Aus der Klinik und Poliklinik für Nuklearmedizin
Klinikum der Ludwig-Maximilians-Universität München

Dissertation

zum Erwerb des Doctor of Philosophy (Ph.D.)

an der Medizinischen Fakultät der

Ludwig-Maximilians-Universität zu München

FET-PET-based radiomics in IDH-wildtype glioblastoma

vorgelegt von:
Zhicong Li

aus:

Xuzhou, Jiangsu, China

Jahr:

2023

Mit Genehmigung der Medizinischen Fakultät der

Ludwig-Maximilians-Universität zu München

First evaluator (1. TAC member): Prof. Dr. Nathalie L. Albert

Second evaluator (2. TAC member): Prof. Dr. Karim-Maximilian Niyazi

Third evaluator: Prof. Dr. Rainer Glaß

Fourth evaluator: Prof. Dr. Kirsten Lauber

Dean: **Prof. Dr. med. Thomas Gudermann**

date of the defense:

28.09.2023

Affidavit

| | Affidavit | |

Li, Zhicong
_____
Surname, first name

I hereby declare, that the submitted thesis entitled:

FET-PET-based radiomics in IDH-wildtype glioblastoma

………………………………………………………………………………………………….

is my own work. I have only used the sources indicated and have not made unauthorised use of services of a third party. Where the work of others has been quoted or reproduced, the source is always given.

I further declare that the dissertation presented here has not been submitted in the same or similar form to any other institution for the purpose of obtaining an academic degree.

Munich, 08.10.2023   Zhicong Li
_____   _____
place, date   Signature doctoral candidate

Confirmation of congruency

LMU LUDWIG-MAXIMILIANS-UNIVERSITÄT MÜNCHEN	Promotionsbüro Medizinische Fakultät	MMRS	

Confirmation of congruency between printed and electronic version of the doctoral thesis

Li, Zhicong

_____
Surname, first name

I hereby declare, that the submitted thesis entitled:

FET-PET-based radiomics in IDH-wildtype glioblastoma

……………………………………………………………………………………………….

is congruent with the printed version both in content and format.

Munich, 08.10.2023

_____
place, date

Zhicong Li

_____
Signature doctoral candidate

Table of content

List of abbreviations

Abbreviation	Meaning
ATRX	Alpha thalassemia/mental retardation syndrome x-linked
AUC	Area under the receiver operating characteristic curve
BTV	Biological tumour volumes
CNS	Central nervous system
CT	Computed tomography
DNA	Deoxyribonucleic acid
EGFR	Epidermal growth factor receptor
[^{18}F]FET	*O*-(2-[^{18}F]-fluoroethyl)-l-tyrosine
GBM	Glioblastoma
MGMT	*O*-6-methylguanine-dna-methyltransferase
MRI	Magnetic resonance imaging
OS	Overall survival
PET	Positron emission tomography
RNA	Ribonucleic acid
ROC	Receiver operating characteristic curve
ROI	Regions of interest
STS	Short-term survivors
SUV	Standardized uptake value
SVM	Support vector machine
TAC	Time-activity curve
TBR	Tumour-to-background ratio
TERC	Telomerase ribonucleic acid component
TERT	Telomerase reverse transcriptase
TERTp	Telomerase reverse transcriptase promoter
TTP	Time-to-peak
WHO	World health organization

List of publications

1. Li, Z., Kaiser, L., Holzgreve, A., Ruf, V. C., Suchorska, B., Wenter, V., Lietke, S., Herms, J., Bartenstein, P., Ruf, V. C., Tonn, J., Unterrainer, M., Albert, N. L. (2021). Prediction of TERTp-mutation status in IDH-wildtype high-grade gliomas using pre-treatment dynamic [(^{18})F]FET PET radiomics. European Journal of Nuclear Medicine and Molecular Imaging, 48(13), 4415-4425. doi:10.1007/s00259-021-05526-6

2. Li, Z., Holzgreve, A., Unterrainer, L. M., Ruf, V. C., Quach, S., Bartos, L. M., Suchorska, B., Niyazi, M., Wenter, V., Herms, J., Bartenstein, P., Tonn, J., Unterrainer, M., Albert, N. L., Kaiser, L. (2022). Combination of pre-treatment dynamic [(^{18})F]FET PET radiomics and conventional clinical parameters for the survival stratification in patients with IDH-wildtype glioblastoma. European Journal of Nuclear Medicine and Molecular Imaging. doi:10.1007/s00259-022-05988-2

Your contribution to the publications

1.1   Contribution to paper I

I am the independent first author of this paper. I was responsible for conceptualization, feature selection and machine learning implementation and application, writing - original draft preparation and writing - review and editing.

1.2   Contribution to paper II

I am the independent first author and corresponding author of this paper. I was responsible for conceptualization, feature selection and machine learning implementation and application, writing - original draft preparation and writing - review and editing.

2.   Introductory summary

2.1   Glioblastoma

Glioblastoma (GBM) is the most common malignant primary brain tumour, accounting for around 57% of all gliomas and 48% of all malignant primary tumour in the central nervous system (CNS) with annual incidence of 1.88–4.71 per 100,000 population (Ostrom, Cote, Ascha, Kruchko, & Barnholtz-Sloan, 2018; Ostrom, Gittleman, et al., 2018). Despite advances in the treatment of GBM including surgery, radiation therapy, chemotherapy and targeted therapy, the overall prognosis has not been favourable and long-term survival is rare (Taphoorn, Sizoo, & Bottomley, 2010). The median survival of patients who receive treatment including standard radiation and chemotherapy with temozolomide after diagnosis is only 14.6 months, and median survival of patients without treatment is 4.5 months (Stupp et al., 2005; Wen & Kesari, 2008). Despite these incremental improvements in short-term survival with time, the 5-year survival rate was still relatively stable, with only 5.8% survival at 5 years after diagnosis (Ostrom, Gittleman, et al., 2018).

2.1.1   TERTp Mutation

Telomeres and related shelterin complex are situated at the ends of linear eukaryotic chromosomes. Telomeres usually consist of hexanucleotide repeats of TTAGGG (5′-3′ of the G-rich strand), the length of which varies considerably in different species, being 10-15 kb in humans. Telomere repeat sequences are mostly double-stranded, but terminate with a single-stranded G-rich 150-200 nucleotide long 3′ tail (Maciejowski & de Lange, 2017; Nandakumar & Cech, 2013; Peng, Mian, & Lue, 2001; Roake & Artandi, 2020). Shelterin is a telomere-specific protein complex that works with DNA-binding and adapters to protect unstable telomeres to inhibit the DNA damage response (O'Sullivan & Karlseder, 2010; Sfeir et al., 2009). The stability of chromosomes and the viability of cells rely on sufficient shelterin binding sites being maintained at each telomere. Telomeres need to have a threshold of tandem repeats to enable shelterin proteins to form protective nucleoprotein structures that prevent triggering DNA damage signals resulting in end-fusions and genomic instability ('end-protection problem') (de Lange, 2009; Maciejowski & de Lange, 2017; Masutomi et al., 2000; Sfeir & de Lange, 2012). Telomeric DNA can be lost as cells proliferate because the DNA replication machinery is unable to replicate DNA ends. This end replication problem is tackled by telomerase, a reverse transcriptase that adds telomeric repeats to the 3′ ends of chromosomes, thus, providing compensation for the loss of terminal sequences (Greider & Blackburn, 1985).

Telomerase is a complex consisting of a catalytic subunit encoded by the telomerase reverse transcriptase (TERT) gene and an internal telomerase RNA component (TERC) (Shay & Wright, 2019). While telomerase remains active in germ and proliferating cells, it is typically repressed in differentiated cells. This repression leads to the gradual shortening of telomeres due to incomplete replication and DNA damage. (Hockemeyer & Collins, 2015; Shay & Wright, 2019). Once telomeres reduce to a critical length and malfunction, the DNA damage response pathway is activated, resulting in cells entering a stage of permanent growth arrest known as replicative senescence. It is believed that senescence is an extremely effective mechanism to halt the proliferation and genetic mutations that arise from DNA replication. Infinite proliferation is one of the charac-

teristics of malignant cells, and normally, tumour cells can escape senescence regulation via telomere stabilization (Hanahan & Weinberg, 2011; Shay & Wright, 2019). Tumours have two mechanisms to stabilize telomeres: reactivation of telomerase to extend telomere length (85-90% of cancers), and homologous recombination between sister chromatids (3-10% of cancers) (Barthel et al., 2017; Holt, Wright, & Shay, 1996).

TERC is commonly expressed in a variety of human cells, whereas the TERT gene is strictly inhibited by repressors and enhancers within the promoter of the gene encoding the catalytic subunit to limit telomerase activity (Surovtseva et al., 2009). Therefore, the activity of telomerase is controlled by TERT, which serves as a rate-limiting factor, and in human cells, induction of TERT is essential for acquiring telomerase activity. (Bodnar et al., 1998). Furthermore, the TERT promoter (TERTp) contains many binding sites for transcriptional activators to regulate TERT activity at the transcriptional level (Leão et al., 2018; L. Liu, Lai, Andrews, & Tollefsbol, 2004).

TERTp result in increased promoter activity in cells (Rachakonda, Hoheisel, & Kumar, 2021). Various tumour lesions with promoter mutations expressed statistically significantly enhanced TERT transcription and telomerase activity (Heidenreich et al., 2014; Huang et al., 2015). TERTp mutations are independently related to older age, advanced clinical stage and worse prognosis in patients with GBM. TERTp mutations have been reported to be related to a low overall survival rate in patients with diffuse astrocytic gliomas in the absence of the isocitrate dehydrogenase gene mutation (IDH-wildtype) (Eckel-Passow et al., 2015; Labussière et al., 2014; Vinagre et al., 2013). Specifically, TERTp mutations without IDH mutation have a poor prognosis than TERTp mutations together with IDH mutation (Batista et al., 2016; Killela et al., 2013; M. Simon et al., 2015). And the presence of TERTp mutations decreases sensitivity of brain cancer to adjuvant radiation and chemotherapy with temozolomide (M. Simon et al., 2015). Therefore, TERTp mutations are essential for the initiation of cancer and the prognosis of individuals (Arita et al., 2013; Killela et al., 2013; Matthias Simon et al., 2015), and the analysis of TERTp mutation status is of growing importance in the evaluation of IDH-wildtype glioma to make clinical treatment decision (Brat et al., 2018; Louis et al., 2020; Rushing, 2021).

2.1.2 Survival Stratification

The World Health Organization (WHO) included mandatory molecular markers in the diagnosis of CNS tumours classification in 2016 and updated them in 2021, which generated a stricter definition of entities with different prognosis (Louis et al., 2016; Louis et al., 2021). Particularly, patients with glioma in the absence of IDH mutation are more likely to have a more unfavourable prognosis (Tan et al., 2020) and based on the WHO 2021 guidelines, the absence of IDH mutation is one of the criteria for confirming, grade 4, glioblastoma diagnosis. Methylation status of the O-6-methylguanine-DNA-methyltransferase (MGMT) promotor aid in the stratification of brain tumour patients according to individual risk status as well (Esteller et al., 2000). But in IDH-wildtype glioblastoma, a tumour type with a poor prognosis, some patients live for multiple years, whereas others are classified as short-term survivors (STS) who die within 12 months after diagnosis, suggesting the potential for further improvements in patient stratification (Van Meir et al., 2010). It is critical for patients to balance life quality with intensive therapy that including radiotherapy and chemotherapy (Pace et al.). Therefore, in addition to established molecular genetic markers, the availability of other prognostic markers and survival stratification beyond neuropathological classification of brain tumours will contribute to further improvement of individual prognosis and patient management.

2.2   [^{18}F]FET PET

O-(2-[^{18}F]-fluoroethyl)-L-tyrosine ([^{18}F]FET) is radiolabelled amino acid analogon, and serve as a tool applied to characterize and assess CNS cancers with positron emission tomography (PET) (Jansen, Suchorska, Wenter, Eigenbrod, Schmid-Tannwald, Zwergal, Niyazi, Drexler, Bartenstein, Schnell, Tonn, Thon, Kreth, & la Fougere, 2014; Jansen, Suchorska, Wenter, Schmid-Tannwald, Todica, Eigenbrod, Niyazi, Tonn, Bartenstein, Kreth, & la Fougere, 2015; Popperl et al., 2007). [^{18}F]FET was first used in the human study about brain tumours in 1999, and then has been approved for imagining of brain tumour in Switzerland (Wester et al., 1999). The advantages of this radioactive component include ease of preparation, high stabilization, rapid absorption in the tumour area and low aggregation in non-tumour tissues (Wester et al., 1999).

After injection of [^{18}F]FET 20 to 40 min, static image data (standard 20-40 minutes summation images) are obtained and normally used for evaluation of brain tumour in accordance with the guidelines of Europe and Germany (Langen et al., 2011; Vander Borght et al., 2006). To quantify the uptake of [^{18}F]FET in tumour and non-tumour tissues, the standardized uptake value (SUV) is commonly used. The SUV is decided by dividing the radioactivity (kBq/ml) in the area by the radioactivity injected per gram of body weight. Tumour uptake, in terms of proportion to healthy tissue, is less variable than tumour SUV and is more suitable for inter-individual comparisons. The reference for background regions of interest (ROI) in the normal cerebral hemisphere, which encompass both grey and white matter on the opposite side of the tumour, is utilized. Physiological brain uptake is determined as the mean of SUVs in that region. Therefore, there are two important parameters: mean and maximum tumour-to-background ratio (TBR$_{mean}$ and TBR$_{max}$). To determine TBR$_{mean}$ and TBR$_{max}$, the mean and maximum SUV of the tumour ROI are divided by the mean SUV of the normal area. The volumes of FET-positive tumour, also known as biological tumour volumes (BTVs), are calculated by a 3D automated outlining process using a cut-off TBR of 1.6 or higher (Jansen, Suchorska, Wenter, Eigenbrod, Schmid-Tannwald, Zwergal, Niyazi, Drexler, Bartenstein, Schnell, Tonn, Thon, Kreth, & la Fougère, 2014; Pauleit et al., 2005). This threshold is established from a pathological investigation conducted on gliomas, where a tumour-to-brain ratio of 1.6 proved to be the most effective criterion for distinguishing tumour from peri-tumoural tissue (Pauleit et al., 2005). It is worth noting that the TBR$_{max}$ in particular depends on the quality of scans, methods of reconstruction as well as post-processing of data. As a result, cut-off values for TBR$_{max}$ from different centres are not fully comparable.

Study suggested that the grading of gliomas based on an early scan performed between 5 to 15 minutes post-injection may be more meaningful (Albert, Winkelmann, Suchorska, Wenter, Schmid-Tannwald, Mille, Todica, Brendel, Tonn, Bartenstein, & la Fougere, 2016). This is because higher-grade gliomas, such as IDH-wildtype gliomas, have been demonstrated to exhibit a high uptake of tracer within the initial 5-15 minutes post-injection, followed by a decreasing time-activity-curve. However, IDH-mutant gliomas typically showed a delayed increase uptake of radiopharmaceutical and the peaks occur at the later time ranges (Jansen et al., 2012; Jansen, Suchorska, Wenter, Eigenbrod, Schmid-Tannwald, Zwergal, Niyazi, Drexler, Bartenstein, Schnell, Tonn, Thon, Kreth, & la Fougère, 2014; Popperl et al., 2007). Conventional TBR$_{max}$ values, however, are evaluated in standard static images which excludes early peak uptake of aggressive gliomas. Hence, TBR$_{max}$ acquired from early summation images demonstrate superior performance in distinguishing low- and high-grade gliomas than standard static images (Albert, Winkelmann, Suchorska, Wenter, Schmid-Tannwald, Mille, Todica, Brendel, Tonn, Bartenstein,

& la Fougere, 2016), which shows that the incorporation of early summation images can characterize gliomas well.

Furthermore, the assessment of *dynamic* [^{18}F]FET PET time-activity curves (TAC) has been proved to generate valuable evidences of the characteristics of tumour (Kunz et al., 2019) with regard to tumour grading or differential diagnosis of other diseases (Galldiks, Langen, & Pope, 2015). High-grade tumours have an early peak followed by a decrease in TAC, but low-grade tumours and non-tumorous lesions show a slowly increasing pattern of uptake (Pöpperl et al., 2007; Weckesser et al., 2005). This different pattern of TAC seems to be a particular property of [^{18}F]FET (Kratochwil et al., 2014). In the case of heterogeneous tumours, different regions may show different patterns of curve, suggesting that localized areas of tumour tissue are more malignant compared to the entire tumour, and that the delayed TAC may indicate the degree of malignancy of the tumour (Kunz et al., 2011; Thon et al., 2015). The TAC of [^{18}F]FET can be described qualitatively as different curve patterns and can also be calculated quantitatively using the slope of the TAC and time-to-peak (TTP) in the late time frames (Ceccon et al., 2017; Jansen, Suchorska, Wenter, Schmid-Tannwald, Todica, Eigenbrod, Niyazi, Tonn, Bartenstein, Kreth, & la Fougère, 2015). In particular, in newly diagnosed gliomas, early TTP is correlated with an aggressive disease process and is predictive of IDH-wildtype status (Suchorska et al., 2018; Vettermann et al., 2019).

2.2.1 [^{18}F]FET PET Clinical Application

It is important to differentiate between primary and secondary brain tumours and non-neoplastic origin of the lesion including haemorrhage, infarction, infections and inflammatory processes. [^{18}F]FET PET contribute to the differential diagnosis, as neoplastic lesions usually have higher levels of FET uptake. A meta-analysis consisting of thirteen studies utilizing [^{18}F]FET PET and involving a total of 462 patients revealed that a TBR threshold of 1.6 or higher and TBR_{max} of 2.1 or higher demonstrated the highest diagnostic efficacy in differentiating primary brain tumours from other diseases with a sensitivity of 82% and specificity of 76%. (Dunet, Rossier, Buck, Stupp, & Prior, 2012). A retrospective study of [^{18}F]FET PET with 393 patients obtained a sensitivity of 87% and a specificity of 68% in detecting brain tumours (Hutterer et al., 2013). Hence, [^{18}F]FET PET plays a valuable role in the initial evaluation of newly diagnosed brain lesions. However, for a definitive pathological characterization of the lesions, histological evaluation of tissue through biopsy remains the gold standard in the majority of cases.

As previously mentioned, the improvement can be achieved in in primary tumours and tumours to distinguish low-grade from high-grade gliomas by using early summation images and *dynamic* [^{18}F]FET PET data (Albert, Winkelmann, Suchorska, Wenter, Schmid-Tannwald, Mille, Todica, Brendel, Tonn, Bartenstein, & la Fougère, 2016; Calcagni et al., 2011), though standard 20-40 minutes summation images does not perform well in this respect (Hutterer et al., 2013). Particularly, IDH mutation status is one of the most important factors in the classification of brain tumours according to the WHO classification of CNS in 2021 (Louis et al., 2021). A study on *dynamic* [^{18}F]FET including 341 patients showed that a short TTP_{min} in dynamic [^{18}F]FET PET data used as predictor of IDH-wildtype status in gliomas. Specifically, the subgroup of patients with non-contrast-enhanced GBM demonstrated improved diagnostic outcomes, which will be helpful in identifying patients with worse prognosis (Vettermann et al., 2019).

A prospective longitudinal study support BTV generated from [^{18}F]FET PET static images as an independent factor in prognosis of brain tumours (Suchorska et al., 2015). Another study including 121 astrocytic high-grade glioma patients showed that TTP$_{min}$ derived from *dynamic* [^{18}F]FET PET can be a non-invasive factor in identification of patients with a poor prognosis (Jansen, Suchorska, Wenter, Schmid-Tannwald, Todica, Eigenbrod, Niyazi, Tonn, Bartenstein, Kreth, & la Fougère, 2015). When the morphological features of MR and the uptake of FET PET are considered together, this facilitates improved diagnostic performance in patients with low-grade glioma (Floeth et al., 2007). In addition, studies of *dynamic* [^{18}F]FET PET indicated that decreasing TAC in *dynamic* [^{18}F]FET PET helps to detect high-risk astrocytic low-grade glioma to avoid undegrading and undertreatment (Jansen, Suchorska, Wenter, Eigenbrod, Schmid-Tannwald, Zwergal, Niyazi, Drexler, Bartenstein, Schnell, Tonn, Thon, Kreth, & la Fougère, 2014; Thon et al., 2015). Thus, it can be seen that *dynamic* [^{18}F]FET PET can provide more prognostic value than static one.

It is challenging for MRI to differentiate between tumour progression or recurrence and treatment-related changes, because an increase of enhancement in MRI without further tumour progression can be observed within first 3 months after radiotherapy and/ or chemotherapy with temozolomide (Brandsma & van den Bent, 2009). This phenomenon is called pseudoprogression and can occur in 15–30% of patients with malignant gliomas (Brandsma, Stalpers, Taal, Sminia, & van den Bent, 2008; Young et al., 2011). [^{18}F]FET PET can yield up to 90% accuracy in the differentiation between early tumour progression and pseudoprogression after radiochemotherapy of GBM (Galldiks, Dunkl, et al., 2015; Kebir et al., 2016). Furthermore, post radiation necrosis has similarities in radiology to tumour progression and has become another relevant clinical problem for neurooncologists (Shah et al., 2013). The potential of [^{18}F]FET PET to distinguish tumour recurrence from treatment-related changes in GBM have been assessed, and compared to conventional MRI (85%), [^{18}F]FET PET can achieve much higher accuracy (93%). (Galldiks, Stoffels, et al., 2015). Similar results that [^{18}F]FET PET performed better than MRI in this respect have been obtained in other studies (Pyka et al., 2018; Rachinger et al., 2005; Werner et al., 2019). The uptake of [^{18}F]FET was also used to predict the treatment response in patients with early glioblastomas to radiochemotherapy, with a 10% reduction in uptake implying a longer progression-free survival than patients whose uptake is stable or increased following postoperative treatment (Galldiks et al., 2012; Piroth et al., 2011). The application of anti-angiogenic drugs, such as bevacizumab, has led to rapid restoration of blood-brain barrier, causing a pseudoresponse in MRI (Vredenburgh et al., 2007). A rapid reduction in contrast enhancement after initiation of treatment is observed with bevacizumab, generating a significantly high response rate. And it has been demonstrated that [^{18}F]FET PET distinguishes between responders and non-responders ahead of MRI alone (Galldiks et al., 2013; Hutterer et al., 2011).

2.3   Radiomics

Medical images of all kinds contain a rich amount of valuable information about the characteristics and progression of diseases. Radiomics makes it possible to select specific features or feature combinations to differentiate similar diseases and to predict treatment response and outcomes by transforming medical images into high-dimensional quantitative features (Gillies, Kinahan, & Hricak, 2016; Lambin et al., 2012). Radiomics image analysis has gained increasing attention since the concept was first introduced in 2012 (Lambin et al., 2012).

Radiomics combines a range of computational techniques, which are employed to solve clinical questions. There are several fundamental steps which constitute a pipeline of radiomics including harvest of data, segmentation of tumours, extraction of features, selection of features as well as establishment of models. Radiomics requires a substantial quantity of images and outcomes by exploring the relationships among them. CT images were first used in radiomic studies due to its good accessibility and its large quantities (Lambin et al., 2012). Then, MR images, PET images and ultrasound images were also included in the study of radiomics. As these medical images come from different machines with different parameters, are reconstructed and processed in different ways and come from different hospitals, it sets obstacles to the conduct of radiomics studies. For PET images, differences in PET scanners, parameters of reconstruction and post-processing of data are the main reason of influence (Galavis, Hollensen, Jallow, Paliwal, & Jeraj, 2010; van Velden et al., 2016; Yan et al., 2015). SUV discretization and respiratory motion also have a considerable impact on textural features (Grootjans et al., 2016; Oliver et al., 2015). Therefore, it is necessary to perform pre-processing on the images derived from different machines to meet the requirements for feature extraction.

Typically, radiomics only analyses images of the lesion area within predefined regions of interest (ROIs), which is due to the time-consuming process associated with studying the entire image. This means that it is important to segment ROIs from the images. There are three segmentation methods including manual, semiautomatic, and automatic segmentation. Due to the lack of standardized criteria (Kumar et al., 2012), manual segmentation is highly variable and also depends on the experience of radiologists who perform the segmentation of ROIs. As semi-automatic and automatic segmentation can improve the consistency of segmented of ROIs and save time, an increasing number of studies are using this approach as an alternative to manual segmentation. In studies of PET, a semi-automatic segmentation method is mostly performed. In the study of FET-positive tumour lesions, for example, the area of the tumour is first roughly outlined and then the ROIs is determined using a cut-off TBR, which is used to determine the BTV in tumours, usually with a TBR of 1.6 or higher (Jansen, Suchorska, Wenter, Eigenbrod, Schmid-Tannwald, Zwergal, Niyazi, Drexler, Bartenstein, Schnell, Tonn, Thon, Kreth, & la Fougère, 2014; Pauleit et al., 2005). However, in other images including CT, MRI and ultrasound, manual segmentation is still the main method, which limited reliability and repeatability of radiomics researches.

Radiomic features are generated from the information contained in the ROIs of images. Pyradiomics is currently the most widely used package for feature extraction in python (van Griethuysen et al., 2017). Radiomic features can be divided into first-order, shape-based and texture features (van Griethuysen et al., 2017). First-order statistics features show the distribution of voxel intensities within ROIs (van Griethuysen et al., 2017). Shape-based features included descriptors of the two-dimensional or three-dimensional size and shape of the ROIs (van Griethuysen et al., 2017). Texture features refer to the texture characteristics of tumour in terms of the interrelationship between three or more pixels (van Griethuysen et al., 2017). In addition, the publication of Image Biomarker Standardization Initiative provides the basis for standardizing feature extraction (Zwanenburg et al., 2020).

During feature extraction, a large number of features is assessed, which, however, contain too many redundant information. To avoid overfitting and to reduce time for modelling, feature selection will be needed before building prediction model. And three feature selection methods are available: filter, wrapper, and embedding (Z. Liu et al., 2019). Filter methods for assessing

features with no involvement of models. Univariate and multivariate methods are both filter methods. Univariate filters sort features according to their quality, and multivariate filter is consisting of a sorter and a subset selector, which considers redundancy when selecting relevant features. The wrapper methods are based on special mechanical learning modelling to find optimal features (Larue, Defraene, De Ruysscher, Lambin, & van Elmpt, 2017), while the embedded approach is to complete the feature selection during the iterative modelling of the training set (Bagherzadeh-Khiabani et al., 2016).

The main purpose of radiomics is to establish prediction models with related features to solve clinical issues. Machine learning modelling methods can be classified as supervised and unsupervised, based on the availability of clinical outcomes. Unsupervised learning classifies data as clusters by summarising similarities among samples. Supervised learning classifiers like linear models, support vector machines as well as random forests are the more popular approach when the outcome is known (Larue et al., 2017). Training and testing are two steps to build models. During the training phase, samples are used in combination with the respective medical labels for training. The loss function is used to find the mathematical relationship between features and labels in the model. During the testing phase, a well-trained model will be tested its prediction ability (Z. Liu et al., 2019). It should be noted that over-fitting of the model may lead to too favourable results. The cross-validation is often utilized as an internal calibration method, using the area under the receiver operating characteristic curve (AUC) of the receiver operating characteristic (ROC) curve to assess models' accuracy (Z. Li et al., 2019; Z. Li et al., 2021). Additionally, when assessing classification models, the predictive capability can be evaluated using AUC, accuracy, sensitivity, and specificity. (Z. Liu et al., 2019).

2.3.1 Radiomics Clinical Application

Since the concept of radiomics was developed, there has been an increasing number of studies focusing on radiomics in the diagnosis and therapy of patients. Here, the main focus is set to the studies of radiomics in brain tumours.

Traditional medical imaging including CT, MRI and PET is already an important criterion in brain tumour grading, but radiomics is hoped to further improve this situation. One study used multiparametric diffusion-weighted imaging, a quantitative MRI technique, to distinguish low- and high-grade gliomas with machine learning approach, and achieved good results in the external testing cohort (Xu et al., 2022). Another study built a support vector machine (SVM) model, based on multiparametric MRI, which showed a high AUC of 0.987 to distinguish WHO grade 2 from grade 3 and 4 brain tumours (Q. Tian et al., 2018). Meanwhile, radiomics also plays a potential role in predicting the molecular genotype of brain tumours, which helps to improve the efficacy of targeted therapies. The study of MRI radiomics can not only distinguish the glioma grade, but also predict the IDH mutation and the 1p/19q codeletion status, respectively (Y. Li et al., 2022). In addition, the role of radiomics derived from MRI to predict TERTp mutation status in brain tumours has been shown by several studies (Fang et al., 2020; Jiang et al., 2020; Park et al., 2021). In glioma, a multiparametric MRI-based radiomics study has successfully established a model to predict the TERTp mutation status (H. Tian, Wu, Wu, & Xu, 2020). Besides, MGMT, alpha thalassemia/mental retardation syndrome x-linked (ATRX) mutation status, epidermal growth factor receptor (EGFR), Ki-67 expression level and p53 status were successfully predicted with models generated from radiomic features (Y. Li, Liu, Qian, et al., 2018; Y. Li, Liu, Xu, et al., 2018; Y. Li, Qian, et al., 2018; Y. Li et al., 2017; Xi et al., 2018).

The prediction of treatment response and prognosis is another hot topic in radiomics. A multicentre study provided a radiomic model, which including diffusion- and perfusion-weighted MRI, to identify pseudoprogression in patients with GBM (Kim et al., 2019). Another study including 172 patients with recurrent GBM before bevacizumab treatment extracted 4,842 quantitative MRI features and then classified patients into a low and high-risk cohort for progression-free and overall survival (OS) with a prediction model derived from supervised principal component analysis (Kickingereder et al., 2016). These studies both demonstrate the non-invasive role of radiomics in clinical treatment decisions. In addition, radiomics can serve as an independent preoperative tool to predict OS of patients with IDH-wildtype gliomas, and this was shown in a study of 142 patients from two centres, which was conducted using the latest WHO 2021 criteria for classification (S. Wang et al., 2021). A multiparametric MRI-based radiomic model also provide a favourable predictive ability on progression-free survival and OS of patients with GBM (B. Wang et al., 2021).

[18F]FET PET-based radiomic analysis has been used to differentiate brain metastasis recurrence and radiation injury in 2017 (Lohmann et al., 2017). And this research group then published another study of [18F]FET PET-based radiomics for the detection of pseudoprogression (Lohmann et al., 2020). Another study utilized radiomics generated from [18F]FET PET/MRI to predict the mutational status of IDH, MGMT, ATRX as well as 1p/19q codeletion status (Haubold et al., 2020). In addition, the assessment of [18F]FET PET radiomics' prognostic significance following re-irradiation was conducted, which may be useful in selecting patients with recurrent GBM who would benefit from re-irradiation (Carles et al., 2021). Notably, however, while standard *static* images (20-40 min post-injection) have been used in studies of [18F]FET PET-based radiomics, no radiomics studies on *dynamic* [18F]FET PET or early summation images (5-15 min post-injection) have been published.

2.4   Aims

In summary, the aim of this thesis was to apply radiomics generated from [18F]FET PET to investigate clinical issues related to the diagnostic and prognostic prediction of brain tumours, particularly IDH-wildtype GBM. Concretely, the aim of paper I was to evaluate the value of radiomics generated from early summation images, standard static images and *dynamic* [18F]FET PET images in predicting the status of TERTp mutation in patients with IDH-wildtype GBM prior to treatment. The aim of paper II was to establish and assess a predictive model that used a combination of clinical data and radiomic features extracted from static and *dynamic* [18F]FET PET data for survival stratification of IDH-wildtype GBM patients.

2.5   Conclusions

In conclusion, this thesis has demonstrated the predictive value of [18F]FET PET-based radiomics in the diagnosis as well as prognosis of glioblastoma. Radiomics based on TTP images generated from *dynamic* [18F]FET PET can predict the prognostically relevant TERTp mutation status in IDH-wildtype GBM patients with high accuracy before treatment (paper I). Furthermore, predictive models using [18F]FET PET-based radiomic features and clinical variables were constructed and validated to identify short-term survival in GBM patients (paper II). The maximum accuracy in detecting patients at risk was achieved with the conjunction of clinical parameters and radiomic features extracted from *dynamic* [18F]FET PET. The results indicate that *dynamic*

[^{18}F]FET PET radiomic features can be incorporated with clinical parameters to improve the diagnostic performance for the stratification of patients beyond currently established prognostic markers.

3. Paper I

ORIGINAL ARTICLE

Prediction of TERTp-mutation status in IDH-wildtype high-grade gliomas using pre-treatment dynamic [18F]FET PET radiomics

Zhicong Li[1] · Lena Kaiser[1] · Adrien Holzgreve[1] · Viktoria C. Ruf[2] · Bogdana Suchorska[3,4] · Vera Wenter[1] · Stefanie Quach[3] · Jochen Herms[2] · Peter Bartenstein[1,5] · Jörg-Christian Tonn[3,5] · Marcus Unterrainer[6] · Nathalie L. Albert[1,5]

Abstract

Purpose To evaluate radiomic features extracted from standard static images (20–40 min p.i.), early summation images (5–15 min p.i.), and dynamic [18F]FET PET images for the prediction of TERTp-mutation status in patients with IDH-wildtype high-grade glioma.

Methods A total of 159 patients (median age 60.2 years, range 19–82 years) with newly diagnosed IDH-wildtype diffuse astrocytic glioma (WHO grade III or IV) and dynamic [18F]FET PET prior to surgical intervention were enrolled and divided into a training ($n = 112$) and a testing cohort ($n = 47$) randomly. First-order, shape, and texture radiomic features were extracted from standard static (20–40 min summation images; TBR_{20-40}), early static (5–15 min summation images; TBR_{5-15}), and dynamic (time-to-peak; TTP) images, respectively. Recursive feature elimination was used for feature selection by 10-fold cross-validation in the training cohort after normalization, and logistic regression models were generated using the radiomic features extracted from each image to differentiate TERTp-mutation status. The areas under the ROC curve (AUC), accuracy, sensitivity, specificity, and positive and negative predictive value were calculated to illustrate diagnostic power in both the training and testing cohort.

Results The TTP model comprised nine selected features and achieved highest predictability of TERTp-mutation with an AUC of 0.82 (95% confidence interval 0.71–0.92) and sensitivity of 92.1% in the independent testing cohort. Weak predictive capability was obtained in the TBR_{5-15} model, with an AUC of 0.61 (95% CI 0.42–0.80) in the testing cohort, while no predictive power was observed in the TBR_{20-40} model.

Conclusions Radiomics based on TTP images extracted from *dynamic* [18F]FET PET can predict the TERTp-mutation status of IDH-wildtype diffuse astrocytic high-grade gliomas with high accuracy preoperatively.

Keywords Radiomics · [18F]FET PET · TERTp-mutation · Glioma

This article is part of the Topical Collection on Oncology - Brain

✉ Nathalie L. Albert
  nathalie.albert@med.uni-muenchen.de

[1] Department of Nuclear Medicine, University Hospital, LMU Munich, Marchioninistr. 15, 81377 Munich, Germany

[2] Center for Neuropathology and Prion Research, LMU Munich, Munich, Germany

[3] Department of Neurosurgery, University Hospital, LMU Munich, Munich, Germany

[4] Department of Neurosurgery, Sana Hospital, Duisburg, Germany

[5] German Cancer Consortium (DKTK), Partner Site Munich, German Cancer Research Center (DKFZ), Heidelberg, Germany

[6] Department of Radiology, University Hospital, LMU Munich, Munich, Germany

 Springer

Introduction

Mutations in the telomerase reverse transcriptase promoter (TERTp), leading to telomerase activation and lengthened telomeres, play an important role in the formation of brain cancer and individual prognosis [1–3]. In diffuse astrocytic high-grade gliomas without mutation of the isocitrate dehydrogenase gene (IDH-wildtype), TERTp mutations are reported to be associated with poor overall survival [4–6]. Molecular genetic analysis of the TERTp-mutation status has therefore gained increasing attention in the clinical routine diagnosis of IDH-wildtype diffuse astrocytic gliomas and will be included in the upcoming glioma WHO classification [7–9].

Molecular imaging using positron emission tomography (PET) with radiolabelled amino acids such as O-(2-[^{18}F]-fluoroethyl)-L-tyrosine ([^{18}F]FET) is a useful tool for the characterization and evaluation of primary brain neoplasms [10–12], and its application in the clinical management of brain tumour patients has been recommended by the Response Assessment in Neuro-Oncology (RANO) Working Group [13–17]. While static image data (standard 20–40 min summation images) are particularly used for the delineation of the tumour extent, the assessment of *dynamic* [^{18}F]FET PET data has been shown to provide additional information about tumour biology [18]. More aggressive gliomas (i.e. high-grade gliomas and/or IDH-wildtype gliomas) were shown to be characterized by a high tracer uptake within the first 5–15 min post injection (p.i.) with subsequent curve decrease, while less aggressive gliomas (i.e. low grade gliomas and/or IDH-mutant gliomas) typically show a slowly increasing [^{18}F]FET uptake with highest values in the later time frames [12, 19, 20]. As the early peak uptake in aggressive gliomas is missed in the standard 20–40 min p.i. summation images, it does not surprise that the maximal tumour-to-background ratio (TBR$_{max}$) evaluation obtained in early summation images (5–15 min p.i.) was reported to perform better than the standard static TBR$_{max}$ values (20–40 min p.i.) for the differentiation between low-grade and high-grade gliomas [17], which led to the suggestion to include these early summation images for a better glioma characterization. Another interesting parameter derived from dynamic [^{18}F]FET PET is the minimal time-to-peak (TTP$_{min}$), which is extracted from the time-activity-curves and was reported to provide prognostic information [21]. Interestingly, an early TTP$_{min}$ was associated with an aggressive disease course in newly diagnosed gliomas and was able to predict an IDH-wildtype status [22, 23]. Yet, in our recently published study investigating [^{18}F]FET uptake characteristics in TERTp mutant and TERTp wildtype glioblastomas, neither the standard TBR$_{max}$ as static parameter nor TTP$_{min}$ as dynamic parameter were associated with the TERTp-mutation status [24].

In recent years, radiomics have been increasingly investigated as a promising non-invasive tool for accurate diagnosis and prognosis assessment by converting medical images into high-dimensional quantitative image features and establishing predictive models [25–32]. However, radiomics have not been applied for the detection of TERTp mutations on [^{18}F] FET PET images so far. Therefore, the aim of this study was to evaluate radiomic features extracted from standard static images (20–40 min p.i.), early summation images (5–15 min p.i.) as well as dynamic [^{18}F]FET PET images for the prediction of the TERTp-mutation status in patients with newly diagnosed IDH-wildtype diffuse astrocytic high-grade glioma.

Materials and methods

Patients

Patients with primary diagnosis of a glioma who had received a pre-treatment dynamic [^{18}F]FET PET scan at the Department of Nuclear Medicine of the LMU Munich between December 2005 and June 2016 were screened for this retrospective study. Inclusion criteria were (1) neuropathologically confirmed IDH-wildtype diffuse astrocytic gliomas (WHO grade III or IV) according to the updated 2016 WHO classification [33], (2) availability of the TERTp-mutation status, and (3) pre-treatment dynamic [^{18}F]FET PET scan (ECAT EXACT HR + , Siemens Healthineers, Inc., Erlangen, Germany Siemens Medical Systems, Inc., Erlangen, Germany). [^{18}F]FET-negative gliomas (tumour-to-background ratio, TBR < 1.6) were excluded. All patients had given written informed consent prior to the PET scan as part of the clinical routine. The retrospective analysis of PET imaging data was approved by the institutional ethics committee (604–16). A total of 61% of the investigated patients (97/159) have been evaluated in a previous study [24].

Histopathology and molecular genetic analysis

Histopathology and molecular genetic analyses were performed at the Institute of Neuropathology, LMU Munich, Germany. All patients initially classified according to the 2007 WHO brain tumour classification [34] were reclassified according to the 2016 WHO classification [33]. The IDH-mutation status and TERTp-mutation status were evaluated according to clinical standard protocols [35, 36].

[^{18}F]FET PET imaging

[^{18}F]FET PET scans were performed at the Department of Nuclear Medicine, LMU Munich, Germany. Images were acquired by using an ECAT EXACT HR + PET scanner

19

(Siemens Healthineers, Inc., Erlangen, Germany) with the standard protocol [11, 37]. Exactly 180 MBq of [^{18}F]FET were injected after a 15-min transmission scan with a ^{68}Ge rotating rod source. After tracer injection up to 40 min post injection in 3-D mode consisting of 16 frames (7×10 s, 3×30 s, 1×2 min, 3×5 min, and 2×10 min) with a reconstructed voxel size of $2.03 \times 2.03 \times 2.43$ mm^3 and matrix size of $128 \times 128 \times 63$, dynamic emission recording was finished. Two-dimensional filtered back-projection reconstruction algorithm using a 4.9-mm Hann Filter was applied for image reconstruction, then corrected for attenuation, decay, dead time, and random and scattered coincidences. When relevant motion was visible in dynamic PET data, a frame-wise correction was performed by using PMOD fusion tool (version 3.5, PMOD Technologies, Zurich, Switzerland) after frame-wise checking for motion.

Segmentation of tumour volumes and brain background

First, a background activity was extracted from a large crescent-shaped volume of interest (VOI) in the contralateral healthy hemisphere as published previously [38]. For tumour segmentation, a VOI was drawn using a TBR-threshold of 1.6 in static 20–40 min p.i. summation images as suggested by Pauleit et al. [39]. All segmentations were processed within the PMOD View tool (version 3.5, PMOD Technologies, Zurich, Switzerland).

Image normalization and TTP image generation

We used the in-house developed software described previously by Kaiser et al. [40] (C + + with integration of the ROOT data analysis framework, version 6.22/08, Cern, Switzerland and ITK segmentation and registration toolkit 4.13.3, National Library of Medicine) to generate voxel-wise parametric images. Then we normalized the image values with the mean background value derived from each image by using the VOI of background to generate early 5–15 min p.i. (TBR$_{5-15}$) and late 20–40 min p.i. (TBR$_{20-40}$) TBR images. For TTP images, time-activity curves (TAC) were extracted from each voxel, which were then classified according to the time frame reaching the peak uptake (i.e. (1) < 5 min, (2) 5–10 min, (3) 10–15 min, (4) 15–20 min, (5) 20–30 min, and (6) 30–40 min). To avoid influence from early blood flush, TTP analyses did not include the first 2.7 min p.i. [40]. In case of a positive late slope (15–40 min p.i.), the TTP was always assigned to group 6.

Radiomic feature extraction

Radiomic features from parametric images were extracted with PyRadiomics (version 3.0.1) [41] as introduced previously by Kaiser et al. [42], and complied with the Imaging Biomarker Standardization Initiative (IBSI) guidelines [43]. Before extraction, images were resampled to isotropic voxels using linear interpolation in PyRadiomics (size $2.03 \times 2.03 \times 2.03$ mm ^{3}). Classes of features extracted from TBR$_{5-15}$, TBR$_{20-40}$, and TTP images included first-order features, shape features, and texture features. No image filters were used. The chosen fixed intensity bin size was set to the average interquartile range divided by 4, which led to 0.18 for TBR$_{5-15}$ images and 0.13 for TBR$_{20-40}$ images [42, 44]. As the smallest time frame duration considered in the TTP categories was 5 min, this was used as the fixed bin width for radiomics calculation of TTP images.

Feature selection

Before feature extraction, a stratified random split was used to assign 70% of the patients to the training cohort ($n = 112$) and the remaining 30% to the testing cohort ($n = 47$), with a balanced distribution of TERTp-wildtype and TERTp-mutation.

Features were standardized as follows: for each feature, we calculated the mean value and the standard deviation. The mean value was subtracted from each individual value, which was then divided by the standard deviation. Feature normalization was computed only in the training cohort and then applied on the testing cohort. Since the number of features was large, we compared the similarity of each feature pair. If the Pearson correlation coefficient (PCC) value of the feature pair was larger than 0.99, we removed one of them. After this process, the number of the features was reduced and each feature was independent to each other. The recursive feature elimination (RFE) based on logistic regression classifier was performed to reduce redundant features and select potential TERTp-mutation related features [45]. Considering the imbalance of comparison groups, we performed the weighted logistic regression in the 'balanced' mode, which gives higher weight to the minority class and lower weight to the majority class and therefore automatically adjusts weights inversely proportional to class frequencies in the input data [46]. Each iteration removes a feature which is considered least important. After stratified split-based 10-fold cross-validation, the area under the receiver operating characteristic curve (AUC) of the model in the training cohort was used to determine the optimal number of features.

Model construction and testing

Logistic regression (LR) models were built to predict the TERTp-mutation status by fitting the selected radiomic features. Each model was generated by using only the radiomic

features extracted from each image (i.e. TBR_{5-15}, TBR_{20-40}, and TTP images) separately. According to the coefficients of selected features generated by the LR models [47], the risk probability of TERTp-mutation was calculated by the following formula:

$$P(y = 1|x;\theta) = \frac{1}{1 + e^{-\theta^T x}}$$

x is the value of selected features, θ is the coefficient of selected features, and θ_0 represents the intercept. In case of $P > 0.5$, TERTp-mutation status was considered as positive by the LR model.

Model testing was applied to the independent testing cohort, which was not involved in the process of model training. The workflow of the process is presented in Fig. 1.

Statistical analysis

To evaluate the model performance, receiver operating characteristic curve (ROC) analysis was performed in the training and testing cohort. The AUC was calculated as quantitative measure to illustrate diagnostic power. The accuracy, sensitivity, specificity, positive predictive value (PPV), and negative predictive value (NPV) were calculated. 95% confidence intervals (CI) were calculated by using a non-parametric bootstrap method, which was repeated 1000 times to get a bootstrap distribution of the results.

Categorical variables or continuous variables were reported as numbers and percentages or as mean and standard deviation. Categorical variables were compared by the χ^2 test, and continuous variables were compared by the Mann–Whitney U test. $P < 0.05$ were considered statistically significant. Statistical analyses were programmed in Python (v. 3.8.5; https://www.python.org/).

Results

Patient characteristics

A total of 159 patients (median age, 60.2 years; range, 19–82 years) were enrolled in this study. Exactly 31 patients (19.50%) were diagnosed with TERTp-wildtype, and 128 patients had TERTp mutation. The clinical characteristics are presented in Table 1. There were no significant differences between the training and testing cohorts with regard to age, sex, WHO grade, and TERTp mutation status, with TERTp-wildtype rates of 19.64% and 19.15%, respectively.

Radiomic feature extraction and selection

In this study, 107 radiomic features of candidates were generated from standard static images (20–40 min p.i.), early summation images (5–15 min p.i.), and dynamic [^{18}F]FET PET images respectively, including first-order statistics, shape-based features, and texture features. After PCC process, 80 TBR_{20-40} features, 83 TBR_{5-15} features, and 91 TTP features were retained. For the TBR_{20-40} model, based on the AUC of the 10-fold cross-validation on the training cohort,
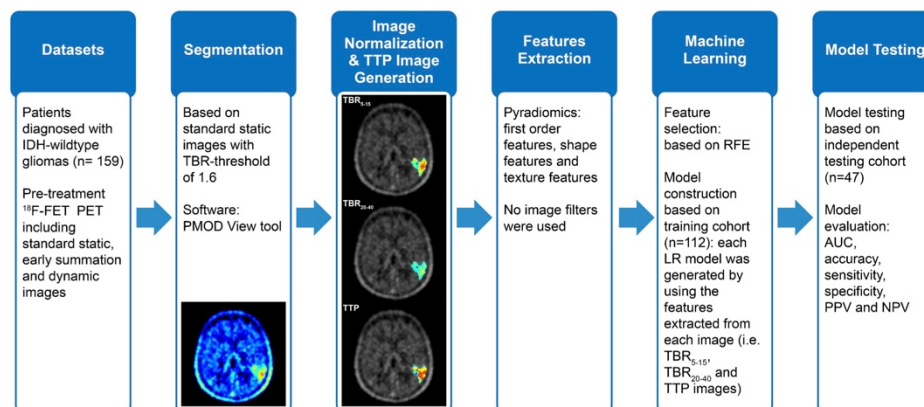
Fig. 1 The workflow of process. TBR tumour-to-background ratio, TTP time-to-peak, RFE recursive feature elimination, LR logistic regression, AUC area under the receiver operating characteristic curve, PPV positive predictive value, NPV negative predictive value

Table 1 Clinical characteristics of the patients

	Training cohort ($n=112$)		Testing cohort ($n=47$)		
	TERTp-mutation	TERTp-wildtype	TERTp-mutation	TERTp-wildtype	P
Characteristic	($n=90$)	($n=22$)	($n=38$)	($n=9$)	0.8958
Age, years	58.1 ± 12.3		59.2 ± 11.2		0.3699
Sex					
Female	45 (40.2%)		17 (54.8%)		0.1449
Male	67 (59.8%)		14 (45.2%)		
WHO grade					
III	39 (34.8%)		14 (29.8%)		0.5389
IV	73 (65.2%)		33 (70.2%)		

Data are means $\pm$ standard deviations or numbers of patients with percentages in parentheses. P value was derived from the univariate association analyses between each clinical parameter. Calculated by using the independent sample t test for continuous variables and the χ^2 test for categoric variables

14 features were finally selected to fit the LR model after performing the RFE method. For the TBR_{5-15} model and the TTP model, 9 features and 10 features were selected for inclusion in the LR model, respectively (Fig. 2).
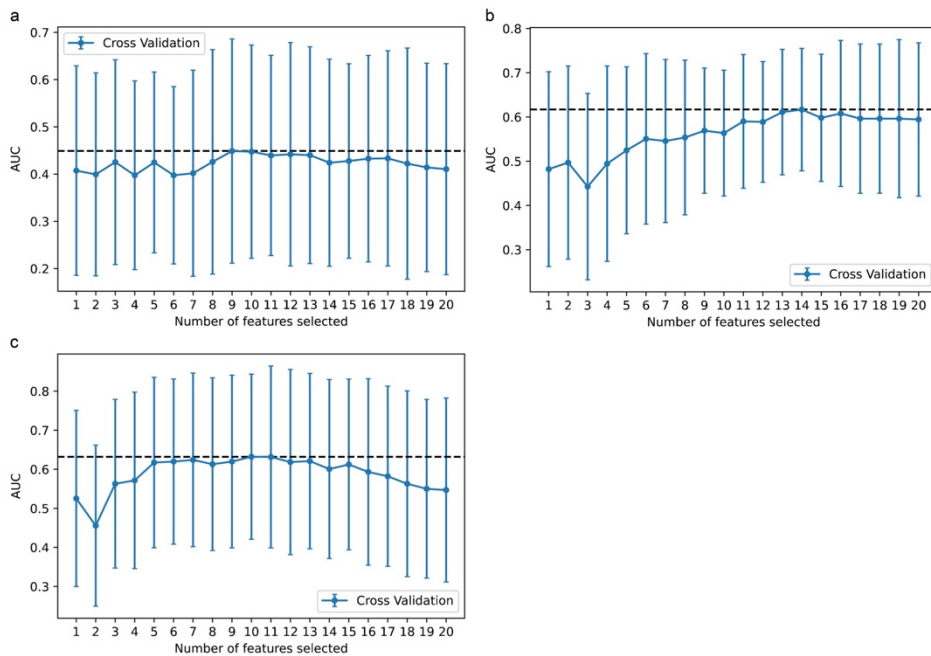
Fig. 2 The feature selection process of the RFE method. Each iteration removes a feature that is considered least important and corresponds to a 10-fold cross-validation. After 10-fold cross-validation, the AUC of the model in the training cohort was used to determine the optimal number of features. The minimum AUC of feature number was selected. **a** TBR_{5-15} model, **b** TBR_{20-40}, and **c** TTP model; 9, 14, and 10 features were selected respectively. RFE recursive feature elimination, AUC area under the receiver operating characteristic curve

Diagnostic Validation of the TBR$_{20-40}$ model, TBR$_{5-15}$ model, and TTP model

According to the above-mentioned formula, the risk probabilities of TERTp-mutation were calculated. The coefficients of selected features in the TBR$_{20-40}$ model and TBR$_{5-15}$ model are shown in Table S1. The coefficients of selected features in the TTP model are shown in Table 2.

No predictive power was observed in the TBR$_{20-40}$ model with an AUC of only 0.49 (95% CI 0.30–0.69) in the testing cohort (AUC of 0.90 in the training cohort (95% CI 0.85–0.95); see Fig. S1). The TBR$_{5-15}$ model demonstrated weak predictive capability to predict a TERTp-mutation (Fig. 3a, b), with an AUC of 0.61 (95% CI 0.42–0.80) in the testing cohort and an AUC of 0.80 (95% CI 0.71–0.89) in the training cohort. The TTP model showed the strongest predictive power and achieved an AUC of 0.82 (95% CI 0.71–0.92) and 0.90 (95% CI 0.84–0.95) in the testing cohort and training cohort, respectively (Fig. 3c, d).

Detailed information about the performance of each model is shown in Table 3.

Discussion

Our study showed that radiomics based on *dynamic* [^{18}F] FET PET data can reliably predict the TERTp-mutation status of IDH-wildtype diffuse astrocytic high-grade gliomas. Best predictability was reached using the TTP model derived from dynamic PET, and weak predictive capability was obtained with radiomics based on early summation images (5–15 min p.i.), while no reliable information about the TERTp-mutation status was possible based on the standard summation images (20–40 min p.i.).

Previous studies have shown that patients with IDH-wildtype TERTp-mutant glioblastoma have a significantly

Table 2 Coefficients of selected features in the TTP model

Features	Coefficients
SmallDependenceLowGreyLevelEmphasis	1.508
Energy	1.404
SmallDependenceHighGreyLevelEmphasis	−1.283
GreyLevelNonUniformityNormalized	−1.235
LeastAxisLength	−1.219
Busyness	−0.916
ShortRunHighGreyLevelEmphasis	−0.699
Maximum2DDiameterColumn	0.654
LowGreyLevelZoneEmphasis	−0.626
LargeDependenceHighGreyLevelEmphasis	0.606

Intercept θ_0 is 0.599 in the TTP model. Details of features were shown in Supplementary Information

shorter progression free and overall survival compared to those with TERT-wildtype status. Therefore, TERTp-mutation status is now considered to be an important diagnostic and prognostic factor in primary glioblastomas and especially in patients with IDH-wildtype glioma [3, 5, 8, 9, 48]. TERTp-mutations indicate tumours that require aggressive and immediate treatments [3]. Hence, a preoperative tool for the prediction of a TERTp-mutation would be useful for early decision making and clinical management of patients with suspected glioma.

Several studies have analyzed the value of MRI based radiomics to predict the TERTp-mutation status in brain tumour patients [49–51]. Although these studies reported to achieve high accuracy values in the range of 79.88–93.80%, only WHO grade II or/and III gliomas have been considered and a limited number of patients has been investigated [49–51]. Besides, Tian et al. established a multiparameter MRI based radiomics model for the prediction of the TERTp-mutation status in patients with high-grade glioma [52], but ignored that TERTp-mutations play different roles in different IDH phenotypes [48].

Compared with conventional MRI, amino acid PET has been shown to be more sensitive in the definition of brain tumour extent [39], and dynamic [^{18}F]FET uptake parameters extracted from the TAC have shown to be an independent biomarker for prognosis [53, 54]. Several studies have reported the informative value of [^{18}F]FET PET-based radiomics in personalized clinical decisions and individualized treatment selection [27–29, 55]. Lohmann et al. found textural feature analysis in combination with TBRs to better differentiate brain metastasis recurrence from radiation injury than TBRs alone, and [^{18}F]FET PET radiomics achieved a higher accuracy than the best standard FET PET parameter (TBR$_{max}$) to diagnose patients with pseudoprogression [27, 55]. Haubold et al. utilized multiparametric [^{18}F]FET PET/MRI and MR fingerprinting to decode and phenotype cerebral gliomas, which may serve as an alternative to invasive tissue characterization [28]. In addition, Carles et al. evaluated the prognostic value of [^{18}F]FET PET radiomics after re-irradiation, and found it could contribute to the selection of recurrent glioblastoma patients benefiting from re-irradiation [29]. However, all studies included radiomics based on standard *static* images (20–40 min p.i.) only and did not extract radiomic features derived from *dynamic* [^{18}F] FET PET as well as early summation images (5–15 min p.i.) even though two studies have shown the impact of *dynamic* parameters on radiomics [32, 56]. Furthermore, no study has evaluated the potential to predict the TERTp-mutation status by [^{18}F]FET PET radiomics so far.

This study included standard static images (20–40 min p.i.), early summation images (5–15 min p.i.), and *dynamic* [^{18}F]FET PET images to develop the radiomic models. A total of 107 features were extracted from each
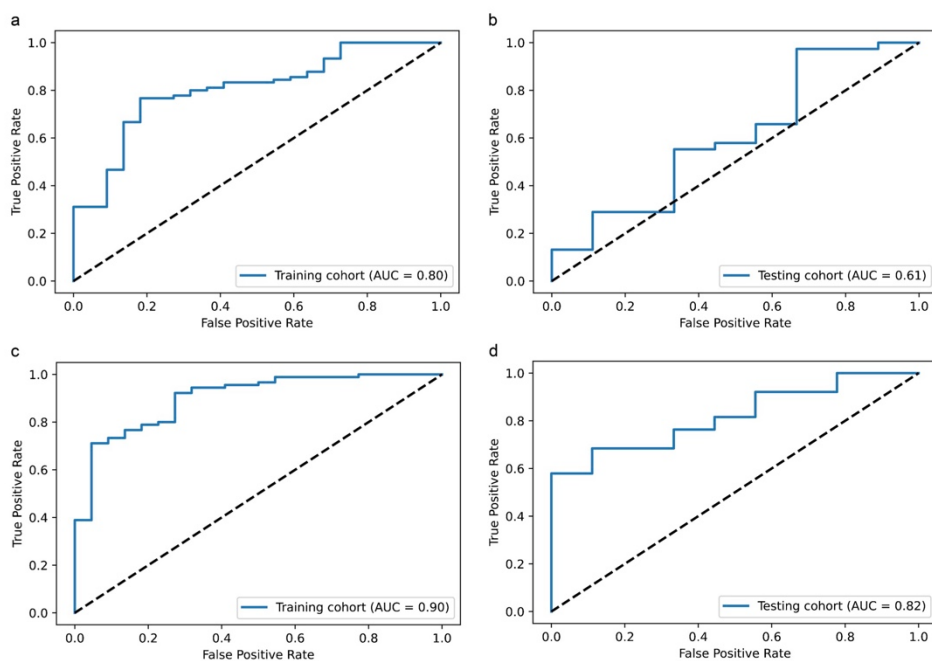
23

Fig. 3 **a** TBR$_{5-15}$ model reached an AUC of 0.80 in the training cohort, and **b** an AUC of 0.61 in the testing cohort. **c** TTP model reached an AUC of 0.90 in the training cohort, and **d** an AUC of 0.82 in the testing cohort. AUC area under the receiver operating characteristic curve

image. Our TTP model, built from ten dynamic [^{18}F] FET PET features selected by RFE, achieved the highest AUC of 0.82 in the independent testing cohort, indicating that the TERTp-mutation status can be predicted by using [^{18}F]FET PET based radiomics. Notably, our former study did neither find an association between the TERTp-mutation status and traditional static [^{18}F] FET PET parameters (TBR$_{max}$ and TBR$_{mean}$ in static 20–40 min summation images) nor the standard dynamic parameter TTP$_{min}$ [24].

Interestingly, radiomics based on the standard TBR$_{20-40}$ model showed a low performance for the prediction of the TERTp-mutation status, and even the TBR$_{5-15}$ model, generated from nine early summation [^{18}F]FET PET features,

Table 3 Performance of each model

	TBR$_{5-15}$		TBR$_{20-40}$		TTP	
	Training cohort	Testing cohort	Training cohort	Testing cohort	Training cohort	Testing cohort
AUC	0.80	0.61	0.90	0.49	0.90	0.82
AUC 95%CI	(0.71–0.89)	(0.42–0.80)	(0.85–0.95)	(0.30–0.69)	(0.84–0.95)	(0.71–0.92)
Accuracy	0.75.0%	66.0%	83.0%	66.0%	78.6%	83.0%
Sensitivity	73.3%	73.7%	81.1%	73.7%	77.8%	92.1%
Specificity	81.8%	33.3%	90.9%	33.3%	81.8%	44.4%
PPV	94.3%	82.4%	97.3%	82.4%	94.6%	87.5%
NPV	42.9%	23.1%	54.1%	23.1%	47.4%	57.1%

CI confidence interval

had an accuracy of only 66% and an AUC of 0.61 in the testing cohort. With a high prediction accuracy of 83% in the TTP model, our study demonstrates that radiomic features extracted from *dynamic* PET data can achieve a higher performance level than models based on static PET data. Remarkably, the sensitivity of the TTP model reached 92.1% in the testing cohort, so that patients with aggressive TERTp-mutant glioma can be identified non-invasively with high probability [3]. With the generated multivariate LR-based formula, health practitioners will be able to calculate the patient individual risk probability of bearing a TERTp-mutation before neurosurgical intervention. Our study shows that even sophisticated radiomic analysis of static [^{18}F]FET PET imaging cannot replace dynamic acquisitions, at least with regard to the prediction of the TERTp-mutation status.

Traditional dynamic [^{18}F]FET PET parameters such as the classification of the time-activity curve (increasing vs. decreasing or increasing vs. plateau vs. decreasing), the slope or the TTP$_{min}$ were most frequently calculated from a mean VOI-TAC of the tumour or from the hot-spot of the tumour with a 90% isocontour [10, 12, 19]. Considering the heterogeneity of gliomas, it may happen that the hot-spot in standard summation images does not correspond to the most suspicious tumour aggressiveness when only considering TTP$_{min}$ and TAC and that, therefore, the most aggressive areas are inadvertently not evaluated. In contrast, we extracted the dynamic [^{18}F]FET uptake information in every voxel within the tumour VOI and generated TTP images. This approach, which was first introduced by Kaiser et al. [40, 42], ensures that the dynamic information including the heterogeneity of uptake kinetics is extracted and that radiomics can be performed on the prognostically valuable dynamic data. The correlation between tumour heterogeneity and TERTp-mutation status can be considered in GreyLevelNonUniformityNormalized (GLNN) feature, which was used in the TTP model (see Table 2). GLNN belongs to Gray Level Dependence Matrix (GLDM), which is mathematically equal to first order–uniformity and is a measure of the homogeneity of the image array. A low value implies a greater heterogeneity, which was correlated with the TERTp-mutation, indicating that tumours with more heterogeneous TTP images are more likely to be classified as TERTp-mutant glioma.

Several limitations of this study should be discussed. First, the number of investigated patients is relatively small. However, it needs to be considered that we analyzed a very homogeneous group of patients with newly diagnosed and untreated IDH-wildtype diffuse astrocytic high-grade glioma. To exclude any influence by scanner type, all images in this study were derived from the same PET scanner, which limited the number of patients as well. In order to increase the number of patients, multi-centre validation studies are needed which, however, require phantom studies and harmonization of reconstruction parameters to make images from different PET scanners comparable. Another approach to directly harmonize features extracted from different devices may be to use the ComBat method [57]. In addition, our results are difficult to extrapolate to other centres, as the PET images analyzed in this study were acquired with our old PET scanner with fixed time frames, resulting in relatively long time frames (predominantly 5 and 10 min) in the dynamic analysis which could not be changed afterwards, and were reconstructed using filtered back-projection, while most PET centres now use other reconstruction methods such as ordered subset expectation maximization (OSEM). Furthermore, radiomic features were only extracted from the [^{18}F]FET-positive tumour VOI to construct the model. Besides the tumour VOI, the remaining image (with normal seeming tissue) may still contain invisible but useful information. To analyze the entire images, deep learning methods will be necessary. Furthermore, our study focused on PET-based radiomics only. A combination with MRI may improve the performance of the prediction model and should be evaluated in future studies.

Conclusion

While conventional [^{18}F]FET PET parameters assessed by standard analyses have previously shown no association with the TERTp-mutation status, radiomic models can predict the TERTp-mutation status of IDH-wildtype diffuse astrocytic high-grade gliomas with high accuracy preoperatively. Notably, this is only the case for radiomics based on *dynamic* image data (TTP model) instead of standard summation images (20–40 min). Further external validation in multi-centre studies with a larger number of patients is needed to evaluate the potential for clinical applications.

Declarations

Ethics approval Ethical approval of the retrospective data analysis was given by the institutional review board of the LMU (# 606–16) in accordance with the ICH Guideline for Good Clinical Practice (GCP) and the Declaration of Helsinki.

Consent to participate All patients have given written informed consent prior to the PET examination.

Consent for publication Not applicable.

Conflict of interest N.L.A. is a member of the Neuroimaging Committee of the EANM. All other authors declare that they have no relationships or interests that could have direct or potential influence or impart bias on the work.

References

1. Arita H, Narita Y, Takami H, Fukushima S, Matsushita Y, Yoshida A, et al. TERT promoter mutations rather than methylation are the main mechanism for TERT upregulation in adult gliomas. Acta Neuropathol. 2013;126:939–41. https://doi.org/10.1007/s00401-013-1203-9.

2. Killela PJ, Reitman ZJ, Jiao Y, Bettegowda C, Agrawal N, Diaz LA Jr, et al. TERT promoter mutations occur frequently in gliomas and a subset of tumors derived from cells with low rates of self-renewal. Proc Natl Acad Sci U S A. 2013;110:6021–6. https://doi.org/10.1073/pnas.1303607110.

3. Simon M, Hosen I, Gousias K, Rachakonda S, Heidenreich B, Gessi M, et al. TERT promoter mutations: a novel independent prognostic factor in primary glioblastomas. Neuro Oncol. 2015;17:45–52. https://doi.org/10.1093/neuonc/nou158.

4. Eckel-Passow JE, Lachance DH, Molinaro AM, Walsh KM, Decker PA, Sicotte H, et al. Glioma groups based on 1p/19q, IDH, and TERT promoter mutations in tumors. N Engl J Med. 2015;372:2499–508. https://doi.org/10.1056/NEJMoa1407279.

5. Labussière M, Di Stefano AL, Gleize V, Boisselier B, Giry M, Mangesius S, et al. TERT promoter mutations in gliomas, genetic associations and clinico-pathological correlations. Br J Cancer. 2014;111:2024–32. https://doi.org/10.1038/bjc.2014.538.

6. Vinagre J, Almeida A, Pópulo H, Batista R, Lyra J, Pinto V, et al. Frequency of TERT promoter mutations in human cancers. Nat Commun. 2013;4:2185. https://doi.org/10.1038/ncomms3185.

7. Rushing EJ. WHO classification of tumors of the nervous system: preview of the upcoming 5th edition. memo - Magazine of European Medical Oncology. 2021. https://doi.org/10.1007/s12254-021-00680-x.

8. Brat DJ, Aldape K, Colman H, Holland EC, Louis DN, Jenkins RB, et al. cIMPACT-NOW update 3: recommended diagnostic criteria for "Diffuse astrocytic glioma, IDH-wildtype, with molecular features of glioblastoma, WHO grade IV." Acta Neuropathol. 2018;136:805–10. https://doi.org/10.1007/s00401-018-1913-0.

9. Louis DN, Wesseling P, Aldape K, Brat DJ, Capper D, Cree IA, et al. cIMPACT-NOW update 6: new entity and diagnostic principle recommendations of the cIMPACT-Utrecht meeting on future CNS tumor classification and grading. Brain Pathol. 2020;30:844–56. https://doi.org/10.1111/bpa.12832.

10. Jansen NL, Suchorska B, Wenter V, Schmid-Tannwald C, Todica A, Eigenbrod S, et al. Prognostic significance of dynamic 18F-FET PET in newly diagnosed astrocytic high-grade glioma. J Nucl Med. 2015;56:9–15. https://doi.org/10.2967/jnumed.114.144675.

11. Jansen NL, Suchorska B, Wenter V, Eigenbrod S, Schmid-Tannwald C, Zwergal A, et al. Dynamic 18F-FET PET in newly diagnosed astrocytic low-grade glioma identifies high-risk patients. J Nucl Med. 2014;55:198–203. https://doi.org/10.2967/jnumed.113.122333.

12. Popperl G, Kreth FW, Mehrkens JH, Herms J, Seelos K, Koch W, et al. FET PET for the evaluation of untreated gliomas: correlation of FET uptake and uptake kinetics with tumour grading. Eur J Nucl Med Mol Imaging. 2007;34:1933–42. https://doi.org/10.1007/s00259-007-0534-y.

13. Albert NL, Weller M, Suchorska B, Galldiks N, Soffietti R, Kim MM, et al. Response assessment in neuro-oncology working group and European Association for Neuro-Oncology recommendations for the clinical use of PET imaging in gliomas. Neuro Oncol. 2016;18:1199–208. https://doi.org/10.1093/neuonc/now058.

14. Langen KJ, Watts C. Neuro-oncology: amino acid PET for brain tumours—ready for the clinic? Nat Rev Neurol. 2016;12:375–6. https://doi.org/10.1038/nrneurol.2016.80.

15. Galldiks N, Langen KJ, Albert NL, Chamberlain M, Soffietti R, Kim MM, et al. PET imaging in patients with brain metastasis-report of the RANO/PET group. Neuro Oncol. 2019;21:585–95. https://doi.org/10.1093/neuonc/noz003.

16. Law I, Albert NL, Arbizu J, Boellaard R, Drzezga A, Galldiks N, et al. Joint EANM/EANO/RANO practice guidelines/SNMMI procedure standards for imaging of gliomas using PET with radiolabelled amino acids and [(18)F]FDG: version 1.0. Eur J Nucl Med Mol Imaging. 2019;46:540–57. https://doi.org/10.1007/s00259-018-4207-9.

17. Albert NL, Winkelmann I, Suchorska B, Wenter V, Schmid-Tannwald C, Mille E, et al. Early static (18)F-FET-PET scans have a higher accuracy for glioma grading than the standard 20–40 min scans. Eur J Nucl Med Mol Imaging. 2016;43:1105–14. https://doi.org/10.1007/s00259-015-3276-2.

18. Kunz M, Albert NL, Unterrainer M, la Fougere C, Egensperger R, Schüller U, et al. Dynamic 18F-FET PET is a powerful imaging biomarker in gadolinium-negative gliomas. Neuro Oncol. 2019;21:274–84. https://doi.org/10.1093/neuonc/noy098.

19. Jansen NL, Graute V, Armbruster L, Suchorska B, Lutz J, Eigenbrod S, et al. MRI-suspected low-grade glioma: is there a need

⚛ Springer

to perform dynamic FET PET? Eur J Nucl Med Mol Imaging. 2012;39:1021–9. https://doi.org/10.1007/s00259-012-2109-9.

20. Jansen NL, Suchorska B, Wenter V, Eigenbrod S, Schmid-Tannwald C, Zwergal A, et al. Dynamic 18F-FET PET in newly diagnosed astrocytic low-grade glioma identifies high-risk patients. J Nucl Med. 2014;55:198–203. https://doi.org/10.2967/jnumed.113.122333.

21. Fleischmann DF, Unterrainer M, Bartenstein P, Belka C, Albert NL, Niyazi M. 18F-FET PET prior to recurrent high-grade glioma re-irradiation—additional prognostic value of dynamic time-to-peak analysis and early static summation images? J Neurooncol. 2017;132:277–86. https://doi.org/10.1007/s11060-016-2366-8.

22. Vettermann F, Suchorska B, Unterrainer M, Nelwan D, Forbrig R, Ruf V, et al. Non-invasive prediction of IDH-wildtype genotype in gliomas using dynamic 18F-FET PET. Eur J Nucl Med Mol Imaging. 2019;46:2581–9. https://doi.org/10.1007/s00259-019-04477-3.

23. Suchorska B, Giese A, Biczok A, Unterrainer M, Weller M, Drexler M, et al. Identification of time-to-peak on dynamic 18F-FET-PET as a prognostic marker specifically in IDH1/2 mutant diffuse astrocytoma. Neuro Oncol. 2018;20:279–88. https://doi.org/10.1093/neuonc/nox153.

24. Unterrainer M, Ruf V, von Rohr K, Suchorska B, Mittlmeier LM, Beyer L, et al. TERT-promoter mutational status in glioblastoma—is there an association with amino acid uptake on dynamic (18)F-FET PET? Front Oncol. 2021;11:645316. https://doi.org/10.3389/fonc.2021.645316.

25. Gillies RJ, Kinahan PE, Hricak H. Radiomics: images are more than pictures, they are data. Radiology. 2016;278:563–77. https://doi.org/10.1148/radiol.2015151169.

26. Lambin P, Rios-Velazquez E, Leijenaar R, Carvalho S, van Stiphout RG, Granton P, et al. Radiomics: extracting more information from medical images using advanced feature analysis. Eur J Cancer. 2012;48:441–6. https://doi.org/10.1016/j.ejca.2011.11.036.

27. Lohmann P, Elahmadawy MA, Gutsche R, Werner JM, Bauer EK, Ceccon G, et al. FET PET radiomics for differentiating pseudoprogression from early tumor progression in glioma patients post-chemoradiation. Cancers (Basel). 2020;12. https://doi.org/10.3390/cancers12123835.

28. Haubold J, Demircioglu A, Gratz M, Glas M, Wrede K, Sure U, et al. Non-invasive tumor decoding and phenotyping of cerebral gliomas utilizing multiparametric (18)F-FET PET-MRI and MR Fingerprinting. Eur J Nucl Med Mol Imaging. 2020;47:1435–45. https://doi.org/10.1007/s00259-019-04602-2.

29. Carles M, Popp I, Starke MM, Mix M, Urbach H, Schimek-Jasch T, et al. FET-PET radiomics in recurrent glioblastoma: prognostic value for outcome after re-irradiation? Radiat Oncol. 2021;16:46. https://doi.org/10.1186/s13014-020-01744-8.

30. Qian J, Herman MG, Brinkmann DH, Laack NN, Kemp BJ, Hunt CH, et al. Prediction of MGMT status for glioblastoma patients using radiomics feature extraction from (18)F-DOPA-PET imaging. Int J Radiat Oncol Biol Phys. 2020;108:1339–46. https://doi.org/10.1016/j.ijrobp.2020.06.073.

31. Lohmann P, Meißner AK, Kocher M, Bauer EK, Fink GR, et al. Feature-based PET/MRI radiomics in patients with brain tumors. Neurooncol Adv. 2020;2:iv15–21. https://doi.org/10.1093/noajnl/vdaa118.

32. Zaragori T, Oster J, Roch V, Hossu G, Chawki MB, Grignon R, et al. (18)F-FDOPA PET for the non-invasive prediction of glioma molecular parameters: a radiomics study. J Nucl Med. 2021. https://doi.org/10.2967/jnumed.120.261545.

33. Louis DN, Perry A, Reifenberger G, von Deimling A, Figarella-Branger D, Cavenee WK, et al. The 2016 World Health Organization Classification of Tumors of the Central Nervous System: a

summary. Acta Neuropathol. 2016;131:803–20. https://doi.org/10.1007/s00401-016-1545-1.

34. Louis DN, Ohgaki H, Wiestler OD, Cavenee WK, Burger PC, Jouvet A, et al. The 2007 WHO classification of tumours of the central nervous system. Acta Neuropathol. 2007;114:97–109. https://doi.org/10.1007/s00401-007-0243-4.

35. Thon N, Eigenbrod S, Kreth S, Lutz J, Tonn JC, Kretzschmar H, et al. IDH1 mutations in grade II astrocytomas are associated with unfavorable progression-free survival and prolonged postrecurrence survival. Cancer. 2012;118:452–60. https://doi.org/10.1002/cncr.26298.

36. Biczok A, Kraus T, Suchorska B, Terpolilli NA, Thorsteinsdottir J, Giese A, et al. TERT promoter mutation is associated with worse prognosis in WHO grade II and III meningiomas. J Neurooncol. 2018;139:671–8. https://doi.org/10.1007/s11060-018-2912-7.

37. Langen KJ, Bartenstein P, Boecker H, Brust P, Coenen HH, Drzezga A, et al. German guidelines for brain tumour imaging by PET and SPECT using labelled amino acids. Nuklearmedizin. 2011;50:167–73. https://doi.org/10.3413/nuk-2011041.

38. Unterrainer M, Vettermann F, Brendel M, Holzgreve A, Lifschitz M, Zahringer M, et al. Towards standardization of 18F-FET PET imaging: do we need a consistent method of background activity assessment? EJNMMI Res. 2017;7:48.

39. Pauleit D, Floeth F, Hamacher K, Riemenschneider MJ, Reifenberger G, Muller HW, et al. O-(2-[18F]fluoroethyl)-L-tyrosine PET combined with MRI improves the diagnostic assessment of cerebral gliomas. Brain. 2005;128:678–87. https://doi.org/10.1093/brain/awh399.

40. Vomacka L, Unterrainer M, Holzgreve A, Mille E, Gosewisch A, Brosch J, et al. Voxel-wise analysis of dynamic 18F-FET PET: a novel approach for non-invasive glioma characterisation. EJNMMI Res. 2018;8:91. https://doi.org/10.1186/s13550-018-0444-y.

41. Van Griethuysen JJM, Fedorov A, Parmar C, Hosny A, Aucoin N, Narayan V, et al. Computational radiomics system to decode the radiographic phenotype. Can Res. 2017;77:e104–7. https://doi.org/10.1158/0008-5472.can-17-0339.

42. Kaiser LGM, Ahmadi SA, Unterrainer M, Holzgreve A, Mille E, Gosewisch A, Brosch J, Suchorska B, Navab N, Tonn JC, Ziegler S, Bartenstein P, Albert NL, Böning G. Annual Congress of the European Association of Nuclear Medicine October 12–16, 2019 Barcelona, Spain. Eur J Nucl Med Mol Imaging. 2019;46:1–952. https://doi.org/10.1007/s00259-019-04486-2.

43. Zwanenburg A, Leger S, Vallières M, Löck S. Image biomarker standardisation initiative. arXiv preprint arXiv:161207003. 2016.

44. Leijenaar RT, Nalbantov G, Carvalho S, van Elmpt WJ, Troost EG, Boellaard R, et al. The effect of SUV discretization in quantitative FDG-PET Radiomics: the need for standardized methodology in tumor texture analysis. Sci Rep. 2015;5:11075. https://doi.org/10.1038/srep11075.

45. Granitto PM, Furlanello C, Biasioli F, Gasperi F. Recursive feature elimination with random forest for PTR-MS analysis of agroindustrial products. Chemometr Intell Lab. 2006;83:83–90. https://doi.org/10.1016/j.chemolab.2006.01.007.

46. Tomz M, King G, Zeng L. ReLogit: rare events logistic regression. 2003. 2003;8:27. https://doi.org/10.18637/jss.v008.i02.

47. Makhoul J. Linear prediction: a tutorial review. Proc IEEE. 1975;63:561–80. https://doi.org/10.1109/PROC.1975.9792.

48. Vuong HG, Altibi AMA, Duong UNP, Ngo HTT, Pham TQ, Chan AK, et al. TERT promoter mutation and its interaction with IDH mutations in glioma: combined TERT promoter and IDH mutations stratifies lower-grade glioma into distinct survival subgroups-A meta-analysis of aggregate data. Crit Rev Oncol Hematol. 2017;120:1–9. https://doi.org/10.1016/j.critrevonc.2017.09.013.

27

49. Jiang C, Kong Z, Zhang Y, Liu S, Liu Z, Chen W, et al. Conventional magnetic resonance imaging-based radiomic signature predicts telomerase reverse transcriptase promoter mutation status in grade II and III gliomas. Neuroradiology. 2020;62:803–13. https://doi.org/10.1007/s00234-020-02392-1.

50. Park CJ, Han K, Kim H, Ahn SS, Choi D, Park YW, et al. MRI features may predict molecular features of glioblastoma in isocitrate dehydrogenase wild-type lower-grade gliomas. AJNR Am J Neuroradiol. 2021;42:448–56. https://doi.org/10.3174/ajnr.A6983.

51. Fang S, Fan Z, Sun Z, Li Y, Liu X, Liang Y, et al. Radiomics features predict telomerase reverse transcriptase promoter mutations in world health organization grade II gliomas via a machine-learning approach. Front Oncol. 2020;10:606741. https://doi.org/10.3389/fonc.2020.606741.

52. Tian H, Wu H, Wu G, Xu G. Noninvasive prediction of TERT promoter mutations in high-grade glioma by radiomics analysis based on multiparameter MRI. Biomed Res Int. 2020;2020:3872314. https://doi.org/10.1155/2020/3872314.

53. Kunz M, Thon N, Eigenbrod S, Hartmann C, Egensperger R, Herms J, et al. Hot spots in dynamic (18)FET-PET delineate malignant tumor parts within suspected WHO grade II gliomas. Neuro Oncol. 2011;13:307–16. https://doi.org/10.1093/neuonc/noq196.

54. Bauer EK, Stoffels G, Blau T, Reifenberger G, Felsberg J, Werner JM, et al. Prediction of survival in patients with IDH-wildtype astrocytic gliomas using dynamic O-(2-[(18)F]-fluoroethyl)-L-tyrosine PET. Eur J Nucl Med Mol Imaging. 2020;47:1486–95. https://doi.org/10.1007/s00259-020-04695-0.

55. Lohmann P, Stoffels G, Ceccon G, Rapp M, Sabel M, Filss CP, et al. Radiation injury vs. recurrent brain metastasis: combining textural feature radiomics analysis and standard parameters may increase (18)F-FET PET accuracy without dynamic scans. Eur Radiol. 2017;27:2916–27. https://doi.org/10.1007/s00330-016-4638-2.

56. Lohmann P, Lerche C, Bauer EK, Steger J, Stoffels G, Blau T, et al. Predicting IDH genotype in gliomas using FET PET radiomics. Sci Rep. 2018;8:13328. https://doi.org/10.1038/s41598-018-31806-7.

57. Orlhac F, Boughdad S, Philippe C, Stalla-Bourdillon H, Nioche C, Champion L, et al. A postreconstruction harmonization method for multicenter radiomic studies in PET. J Nucl Med. 2018;59:1321–8. https://doi.org/10.2967/jnumed.117.199935.

🙆 Springer

28

4. Paper II

ORIGINAL ARTICLE

Combination of pre-treatment dynamic [18F]FET PET radiomics and conventional clinical parameters for the survival stratification in patients with IDH-wildtype glioblastoma

Zhicong Li[1] · Adrien Holzgreve[1] · Lena M. Unterrainer[1] · Viktoria C. Ruf[2] · Stefanie Quach[3] · Laura M. Bartos[1] · Bogdana Suchorska[3,4] · Maximilian Niyazi[5,6] · Vera Wenter[1] · Jochen Herms[2] · Peter Bartenstein[1,6] · Joerg-Christian Tonn[3,6] · Marcus Unterrainer[7] · Nathalie L. Albert[1,6] · Lena Kaiser[1]

Abstract

Purpose The aim of this study was to build and evaluate a prediction model which incorporates clinical parameters and radiomic features extracted from static as well as dynamic [18F]FET PET for the survival stratification in patients with newly diagnosed IDH-wildtype glioblastoma.

Methods A total of 141 patients with newly diagnosed IDH-wildtype glioblastoma and dynamic [18F]FET PET prior to surgical intervention were included. Patients with a survival time ≤ 12 months were classified as short-term survivors. First order, shape, and texture radiomic features were extracted from pre-treatment static (tumor-to-background ratio; TBR) and dynamic (time-to-peak; TTP) images, respectively, and randomly divided into a training ($n=99$) and a testing cohort ($n=42$). After feature normalization, recursive feature elimination was applied for feature selection using 5-fold cross-validation on the training cohort, and a machine learning model was constructed to compare radiomic models and combined clinical-radiomic models with selected radiomic features and clinical parameters. The area under the ROC curve (AUC), accuracy, sensitivity, specificity, and positive and negative predictive values were calculated to assess the predictive performance for identifying short-term survivors in both the training and testing cohort.

Results A combined clinical-radiomic model comprising six clinical parameters and six selected dynamic radiomic features achieved highest predictability of short-term survival with an AUC of 0.74 (95% confidence interval, 0.60–0.88) in the independent testing cohort.

Conclusions This study successfully built and evaluated prediction models using [18F]FET PET-based radiomic features and clinical parameters for the individualized assessment of short-term survival in patients with a newly diagnosed IDH-wildtype glioblastoma. The combination of both clinical parameters and dynamic [18F]FET PET–based radiomic features reached highest accuracy in identifying patients at risk. Although the achieved accuracy level remained moderate, our data shows that the integration of dynamic [18F]FET PET radiomic data into clinical prediction models may improve patient stratification beyond established prognostic markers.

Keywords Radiomics · [18F]FET PET · Survival · Glioma

Introduction

The inclusion of mandatory molecular markers for diagnosis in the World Health Organization (WHO) Classification of Tumors of the Central Nervous System (CNS) in 2016 and revised in 2021 has led to a more rigid definition of prognostically distinct entities [1, 2]. In particular, the isocitrate dehydrogenase (IDH)-wildtype status is associated with a worse prognosis in adult diffuse astrocytic gliomas [3] and results in the diagnosis of a glioblastoma, WHO grade

Nathalie L. Albert and Lena Kaiser contributed equally to this work.

This article is part of the Topical Collection on Oncology - Brain.

✉ Zhicong Li
lzc1225@163.com

Extended author information available on the last page of the article

⚛ Springer

4, according to the 2021 WHO classification. Additional predictive markers such as the methylation status of the O-6-methylguanine-DNA-methyltransferase (MGMT) promotor further help to stratify brain tumor patients according to their individual risk profile [4]. However, even within the distinct molecularly defined tumor type of IDH-wildtype glioblastomas, few patients survive several years whereas others remain short-term survivors (STS) and decease within the first year, indicating further potential for improvement regarding patient stratification [5]. Balancing aggressive treatment including radiation and chemotherapy with quality of life is critical for patients [6].Therefore, additional prognostic markers beyond established molecular genetic markers and a stratification of survival beyond the neuropathological classification of brain tumors would be helpful to further improve individual prognostication and guide patient management accordingly.

Molecular imaging using positron emission tomography (PET) with radiolabeled amino acids such as O-(2-[^{18}F]-fluoroethyl)-L-tyrosine ([^{18}F]FET) has been applied successfully for the characterization and evaluation of primary brain neoplasms [7–9]. Hence, PET imaging was recommended by the Response Assessment in Neuro-Oncology (RANO) Working Group as useful imaging method in addition to conventional magnetic resonance imaging (MRI) in the clinical management of brain tumor patients [10]. Especially dynamic [^{18}F]FET PET has been shown to be helpful for non-invasive tumor classification [11] and for individual prognostication even within defined molecular subgroups [7, 12]. Here, radiomics have recently gained increasing interest as a promising non-invasive tool, where quantitative features are extracted from medical images and combined with clinical and genomic information to establish predictive models [13, 14]. However, up to now, there is no radiomic approach based on dynamic [^{18}F]FET PET data which aims to perform survival stratification in patients with an IDH-wildtype glioblastoma, despite being one of the most common and aggressive brain tumors.

Therefore, the purpose of this study was to build and evaluate a prediction model, which incorporates clinical parameters and radiomic features extracted from static as well as dynamic [^{18}F]FET PET for an individualized survival stratification in patients with a newly diagnosed IDH-wildtype glioblastoma.

Materials and methods

Patients

The retrospective analysis of PET imaging and clinical data was approved by the institutional review board of the LMU Munich (604–16), and all patients gave written informed consent before the PET scan. Patients with primary diagnosis of a glioma who received a pre-treatment dynamic [^{18}F]FET PET scan at the Department of Nuclear Medicine of the LMU Munich were identified for this retrospective study. The inclusion criteria for analysis were (1) histologically confirmed IDH-wildtype glioblastoma according to the updated 2016 WHO classification [1]; (2) pre-treatment evaluation of a dynamic [^{18}F]FET PET scan (ECAT EXACT HR +, Siemens Healthineers, Inc., Erlangen, Germany; Siemens Medical Systems, Inc., Erlangen, Germany); (3) [^{18}F]FET-positive glioma (tumor-to-background ratio, TBR $\geq$ 1.6); and (4) availability of clinical characteristics, including age, gender, Karnofsky Performance Score (KPS), as well as MGMT promoter methylation status and telomerase reverse transcriptase promoter (TERTp) mutation status. Patients with no follow-up data were excluded. Patients with a survival time $\leq$ 12 months were defined as short-term survivors (STS) [15, 16].

[^{18}F]FET PET image acquisition

[^{18}F]FET PET images were acquired on an ECAT EXACT HR + PET scanner (Siemens Healthineers) with the standard protocol [8, 17] at the Department of Nuclear Medicine of the LMU Munich. Dynamic [^{18}F]FET PET images were acquired over 40 as detailed in [14]. If relevant motion was observed in dynamic PET images, a frame-wise correction was performed using PMOD fusion tool (version 3.5; PMOD Technologies, Zurich, Switzerland) after frame-wise checking for motion.

Segmentation of tumor volumes and brain background

The mean background activity was assessed from a large crescent-shaped volume of interest (VOI) in the contralateral healthy hemisphere as published previously [18] and recommended in the Joint EANM/EANO/RANO practice guidelines/SNMMI procedure standards for imaging of gliomas using PET with radiolabeled amino acids [19]. For tumor segmentation, a VOI was delineated with a TBR-threshold of 1.6 in static 20–40 min p.i. summation images as previously described [20].

TBR and TTP image generation

The image values were normalized with the mean background value to generate static 20–40 min p.i. (TBR$_{20–40}$) TBR images. An in-house developed software described previously by Kaiser et al. [21] (C + + with integration of the ROOT data analysis framework, version 6.22/08, CERN, Switzerland; and ITK segmentation and registration toolkit 4.13.3, National Library of Medicine, National Institutes of

Health, USA) was applied to generate voxel-wise parametric images. For the generation of TTP images, time–activity curves (TACs) were derived from each voxel, which were then classified according to the time frame reaching the peak uptake, i.e., (1) < 5 min, (2) 5–10 min, (3) 10–15 min, (4) 15–20 min, (5) 20–30 min, and (6) 30–40 min. TTP analyses excluded the first 2.7 min p.i. to avoid influence from early blood flush [21]. In case of a positive late slope (15–40 min p.i.), the TTP was assigned to group 6.

Radiomic feature extraction

Images were resampled to isotropic voxels using linear interpolation (size $2.03 \times 2.03 \times 2.03$ mm^3), then radiomic features were extracted in Python (version 3.8.5) using PyRadiomics (version 3.0.1) [22], which complies with the Imaging Biomarker Standardization Initiative (IBSI) guidelines [23]. The included feature classes were first-order features, shape features and texture features, which were extracted from TBR and TTP images, respectively. No image filters were applied. As previously published, a fixed intensity bin size was set to 0.13 for TBR$_{20-40}$ images, resulting from the average interquartile range divided by 4 [21, 24, 25]. The smallest time frame duration considered in the TTP categories was 5 min, which was used as the fixed bin width for feature extraction from TTP images.

Machine learning pipeline

Before feature selection, a stratified random split was used to assign 70% of the patients to the training cohort ($n = 99$)

and the remaining 30% to the testing cohort ($n = 42$), with a balanced distribution of STS and non-STS ($P = 0.8654$, Pearson's χ^2 test) and clinical parameters in both groups using the FeAture Explorer (FAE) [26]. The independent testing cohort was not involved in the process of model training and used only for model testing. Machine learning including feature selection and model construction was implemented in Python (version 3.8.5) using scikit-learn package (version 0.24.1) [27]. The workflow of the processing pipeline is presented in Fig. 1.

Feature standardization was computed only on the training cohort and then applied to both the training and the testing cohorts. For each feature, the mean value and the standard deviation were calculated. The mean value was subtracted from each individual value, which was then divided by the standard deviation.

Before performance evaluation on the test set, feature selection and model fitting was conducted on the training set. Logistic regression (LR) models were built to predict short-term survival of GBM patients in the testing cohort by fitting selected features on the training cohort. For survival classification, LR was applied in "balanced" mode, which gives higher weight to the minority class and lower weight to the majority class. With this setting, weights are automatically adjusted inversely proportional to class frequencies in the input data to avoid the influence from the imbalance of comparison groups [28]. Considering the small amount of data, the solver "liblinear" was used and the maximum number of iterations was set to 1000 for the solver to converge. The remaining settings of the logistic regression classifier provided within the scikit-learn package were set to default.
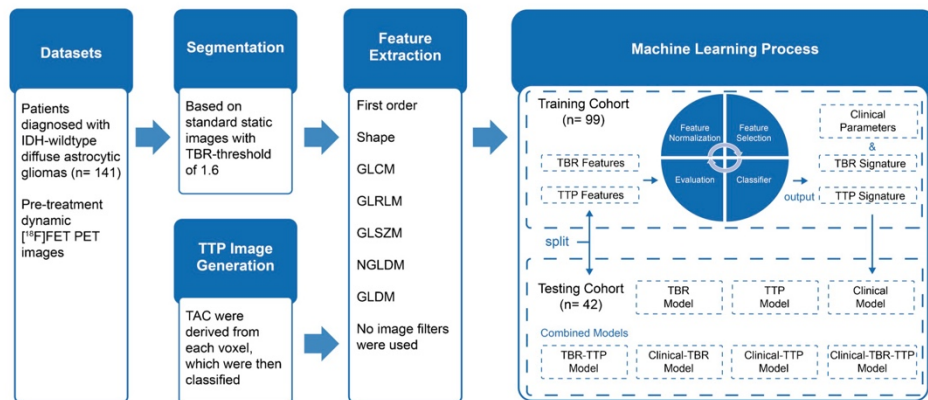

Fig. 1 The workflow of radiomic process. TBR, tumor-to-background ratio; TTP, time-to-peak; TAC, time–activity curves; GLCM, gray level co-occurrence matrix; GLRLM, gray level run length; GLSZM, gray level size-zone matrix; NGLDM, neighborhood gray level different matrix; GLDM, gray level dependence matrix

31

Radiomic feature selection

Pearson correlation coefficient (PCC) was used to reduce the dimensions of the feature matrix [29]. The PCC of two features was compared iteratively. If the PCC was larger than 0.99 [30], the second feature was removed. Furthermore, recursive feature elimination (RFE) based on logistic regression classifier was performed to reduce the number of redundant features and select potential survival-related features [31]. During each iteration, a feature which is considered least important is deleted. The number of features to select was chosen to range between 1 and 15. The performance of each model with a different number of features was assessed using the area under the receiver operating characteristic curve (AUC) obtained from repeated stratified cross-validation using three splits and five folds.

Model construction and testing

First, models considering radiomic features derived from either TBR or TTP images or only clinical parameters were generated and compared to each other. Radiomic signatures were generated by using linear combinations of the selected radiomic features according to the LR coefficients in the TBR and TTP models. The clinical model was constructed from all clinical parameters including age, gender, KPS, MGMT promoter methylation status, and TERTp mutation status. Second, the TBR-TTP model was built from a combination of the TBR signature and the TTP signature. The combined clinical-radiomic models were constructed by combining clinical parameters and radiomic signatures, respectively.

Statistical analysis

Receiver operating characteristic curve (ROC) analysis was performed on the training and testing cohorts to evaluate the model performance. AUC, accuracy, sensitivity, specificity, positive predictive value (PPV), and negative predictive value (NPV) were calculated for diagnostic power when applying the trained model on the testing cohort. Then, 95% confidence intervals (CIs) were calculated by using a non-parametric bootstrap method, which was repeated 1000 times to get a bootstrap distribution of the results.

Categorical variables or continuous variables were reported as numbers and percentages or as mean and standard deviation. Categorical variables were compared using Pearson's χ^2 test and continuous variables were compared using Mann–Whitney U test. P values < 0.05 were considered statistically significant.

Statistical analyses were implemented in Python (version 3.8.5) using scikit-learn package (version 0.24.1) [27].

Results

Patient characteristics

A total of 141 patients (median age, 59.3 years; range, 19.0–77.2 years) were included in this study. Of the 141 patients, 94 (66.7%) patients underwent stereotactic biopsy and 47 (33.3%) microsurgical resection at initial diagnosis, with the same distribution between the training and testing cohorts and no significant differences between both STS and non-STS group (P value = 0.355). Forty patients (28.4%) had a survival time of less than 12 months and were classified as STS. The variables which constructed the clinical model included age, gender, Karnofsky Performance Score, CNS WHO grade, MGMT promoter methylation status, and TERTp mutation status, and are presented in Table 1. There were no significant differences between the training and testing cohorts with regard to clinical parameters, with STS rates of 28.3% and 28.6%, respectively. The initial therapies of STS and non-STS are shown in Table S1.

Radiomic feature extraction and selection

The original features considered for the model construction included six clinical parameters and 107 radiomic features extracted from static and dynamic [18F]FET PET images, respectively. After the PCC-based exclusion of redundant features, 79 features were retained from TBR images and 94 features were retained from TTP images. With RFE, two features were finally selected for the TBR model and six features for the TTP model (Fig. 2).

Diagnostic validation of the TBR model, TTP model, and clinical model

The TBR model reached an AUC of 0.63 (95% CI, 0.52–0.75) in the training cohort for the prediction of STS (Supplementary Fig. S1a, S1b), with a sensitivity of 60.7% and a specificity of 60.6%, and a similar AUC of 0.63 (95% CI, 0.47–0.78) in the testing cohort, with a sensitivity of 50.0% and a specificity of 73.3%. The TTP model showed a higher predictability of STS (Fig. S1c, S1d) with an AUC of 0.77 (95% CI, 0.69–0.84) in the training cohort (sensitivity 75.0% and specificity 63.4%), and with an AUC of 0.71 (95% CI, 0.57–0.84) in the testing cohort (sensitivity 50.0% and specificity 70.0%). The clinical model demonstrated an accuracy at a comparable level as the TTP model (Fig. S1e, S1f), with an AUC of 0.79 (95% CI, 0.71–0.86) in the training cohort (sensitivity 75.0% and specificity 64.8%) and an AUC of 0.69 (95% CI, 0.50–0.86) in the testing cohort (sensitivity 66.7% and specificity 53.3%).

The coefficients of features in the clinical model are shown in Supplementary Table S2. Radiomic signatures are

Table 1 Clinical characteristics of the patients

	Training cohort ($n=99$)		Testing cohort ($n=42$)		P value
	STS	Non-STS	STS	Non-STS	
Characteristic	($n=28$)	($n=71$)	($n=12$)	($n=30$)	0.865
Age, years	56.7 ± 11.8		58.5 ± 13.1		0.121
Gender					
Female (0)	40 (40.4%)		17 (40.5%)		0.857
Male (1)	59 (59.6%)		25 (59.4%)		
KPS	80 (60–100)		80 (40–100)		0.587
WHO grade					
III	32 (32.3%)		16 (38.1%)		0.640
IV	67 (67.7%)		26 (61.9%)		
MGMT					
Unmethyl. (0)	47 (53.0%)		20 (51.2%)		0.988
Methyl. (1)	52 (47.0%)		22 (48.8%)		
TERTp					
Wildtype (0)	21 (21.2%)		10 (23.8%)		0.516
Mutation (1)	78 (78.8%)		32 (76.2%)		

Data are means $\pm$ standard deviations or numbers of patients with percentages in parentheses. P value was derived from the univariate association analyses between each clinical parameter. Calculated by using the Mann–Whitney U test for continuous variables and Pearson's χ^2 test for categoric variables. Gender, MGMT, TERTp with representative number of formula of risk probability in parentheses

STS short-term survivors, *KPS* Karnofsky Performance Score
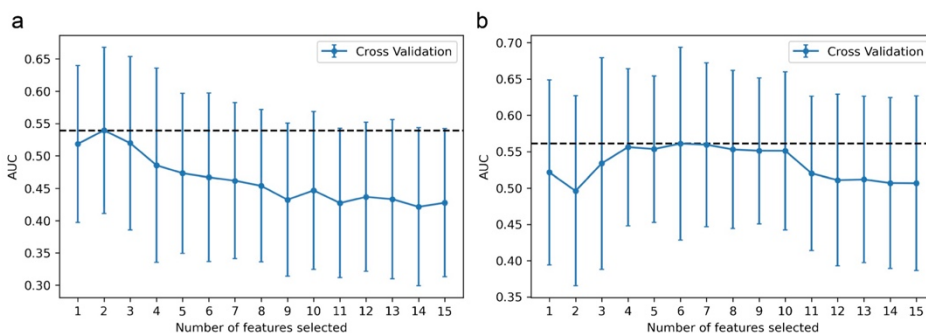
Fig. 2 The feature selection process of the RFE. Each iteration removes a feature that is considered least important and corresponds to a 3-repeated 5-fold cross-validation. After cross-validation, the average AUC of the model in the training cohort was used to determine the optimal number of features. The number of candidate features was chosen to range from 1 to 15. The feature number with maximal AUC was selected. **a** Two features were selected in the TBR model and **b** six features were selected in the TTP model. RFE, recursive feature elimination; AUC, area under the receiver operating characteristic curve

provided in Supplementary section S2. Detailed information about the performance of the different models is shown in Table 2 and Supplementary Table S3.

Diagnostic validation of the combination models

The combined TBR-TTP model reached an AUC of 0.79 (95% CI, 0.72–0.87) in the training cohort for the prediction

Table 2 Performance of TBR, TTP, and clinical models for the testing cohort

	TBR model	TTP model	Clinical model
AUC	0.63	0.71	0.69
AUC 95% CI	(0.47–0.78)	(0.57–0.84)	(0.50–0.86)
Accuracy	66.7%	64.3%	57.1%
Sensitivity	50.0%	50.0%	66.7%
Specificity	73.3%	70.0%	53.3%
PPV	42.9%	40.0%	36.4%
NPV	78.6%	77.8%	80.0%

CI confidence interval, *TBR* tumor-to-background ratio, *TTP* time-to-peak

of STS (Supplementary Fig. S2a, S2b), with a sensitivity of 71.4% and a specificity of 69.0%, and an AUC of 0.74 (95% CI, 0.61–0.86) in the testing cohort, with a sensitivity of 50.0% and a specificity of 70.0%.

The combined clinical-TBR model showed only slightly higher predictability of STS than the TBR model, with an AUC of 0.80 (95% CI, 0.72–0.87) in the training cohort and 0.64 (95% CI, 0.47–0.81) in the testing cohort (Fig. S2c, S2d). The sensitivity and specificity were 75.0% and 70.4% in the training cohort, and 58.3% and 60.0% in the testing cohort, respectively.

The combined clinical-TTP model showed best predictability of STS, with an AUC of 0.86 (95% CI, 0.78–0.92) in the training cohort (sensitivity 82.1% and specificity 74.7%) and 0.74 (95% CI, 0.60–0.88) in the testing cohort (sensitivity 66.7% and specificity 70.0%) (Fig. S2e, S2f).

The clinical-TBR-TTP model reached an AUC of 0.86 (95% CI, 0.70–0.93) in the training cohort for the prediction of STS (Fig. S2g, S2h), with a sensitivity of 89.3% and a specificity of 71.8%, and AUC of 0.72 (95% CI, 0.59–0.86) in the testing cohort, with a sensitivity of 58.3% and a specificity of 73.3%.

LR coefficients of the combined models are provided in Supplementary section S3. Detailed information about the performance of the combined models is shown in Table 3 and Supplementary Table S4.

Discussion

This study illustrates that integration of radiomics based on dynamic [18F]FET PET may improve the assessment of short-term survival probability in patients with newly diagnosed IDH-wildtype glioblastoma. As opposed to prediction models based on clinical parameters or radiomic features alone, specifically a combined clinical-TTP model including both clinical parameters and an additional radiomic signature derived from dynamic PET accomplished a higher prognostic value for short-term survival.

Several studies have analyzed the role of [18F]FET PET for the assessment of survival probability in patients with glioma [7, 8, 12, 32–35]. It has been reported that a large biological tumor volume (BTV) on static [18F]FET PET [32, 33, 35] as well as a short TTP_{min} extracted from dynamic [18F]FET PET at initial diagnosis are associated with STS [7, 12, 34, 35]. Besides, Bauer et al. showed that TTP_{min} is an independent prognostic factor for overall survival, reaffirming the value of dynamic [18F]FET PET in the prediction of survival in glioma patients. Yet, initial radiomics data in high-grade glioma have been provided by MRI studies, achieving high AUC values for the prognostication of overall survival in the range of 0.652–0.858 in the test cohort [36–40] demonstrating that radiomics might be a valuable tool to estimate survival in brain tumor patients. Meanwhile, first promising studies have brought [18F]FET PET–based radiomics into the focus: Radiomic features extracted from static [18F]FET PET showed better accuracy than conventional static parameters (e.g., TBR_{max}) to identify pseudoprogression [13]. For the differentiation between radiation injury and recurrence of brain metastasis, textural features extracted from [18F]FET PET had a diagnostic accuracy of 83% [41]. Carles et al. reported that [18F]FET PET radiomics could contribute to the prognostic assessment [42], and Paprottka et al. established a promising tool for objective differentiation of tumor progression from treatment-related changes by combining [18F]FET PET and multiparametric MRI [43]. However, those initial studies only analyzed static [18F]FET PET features without taking into account important clinical parameters and, furthermore, no study so far has

Table 3 Performance of combined models for the testing cohort

Model	AUC	95% CI	Accuracy (%)	Sensitivity (%)	Specificity (%)	PPV (%)	NPV (%)
TBR-TTP	0.74	(0.61–0.86)	64.3	50.0	70.0	40.0	77.8
Clinical-TBR	0.64	(0.47–0.81)	59.5	58.3	60.0	36.8	78.3
Clinical-TTP	0.74	(0.60–0.88)	69.0	66.7	70.0	47.1	84.0
Clinical-TBR-TTP	0.72	(0.59–0.86)	69.0	58.3	73.3	46.7	81.5

CI confidence interval, *TBR* tumor-to-background ratio, *TTP* time-to-peak

34

utilized dynamic [^{18}F]FET PET–based radiomics to assess the probability of poor prognosis within distinct molecular brain tumor types.

The present study used clinical parameters combined with [^{18}F]FET PET radiomic features to develop combined clinical-radiomic models. A model based on clinical data only, built from six important survival-related clinical parameters, achieved an AUC of 0.69 in the independent testing cohort. A TBR model, built from two static [^{18}F] FET PET features, achieved an AUC of 0.63 in the testing cohort and thus did not perform better than the clinical model. The TTP model, however, generated from six dynamic [^{18}F]FET PET features, achieved an AUC of 0.71 in the testing cohort, thus slightly exceeding the clinical-only model and outranging the TBR-only model, highlighting the importance of dynamic PET data in the context of survival-related analyses. The combined purely imaging-based TBR-TTP model achieved only slightly better results than each model alone (AUC of 0.74 vs. AUC of 0.63 and AUC of 0.71). Eventually, the merger of the TTP radiomic signature and clinical data, resulting in the combined clinical-TTP model, achieved best predictive performance with an AUC of 0.74. Integrated discrimination improvement (IDI) was calculated between the clinical model and the combined clinical-TTP model [44]. The value of IDI was 0.1089, which was greater than 0, and the P value was 0.023, which was statistically significant. It indicated that the combination of TTP radiomics and clinical data, compared to clinical parameters alone, led to an improved ability of the model to identify patients at risk. Although intriguing to speculate that the clinical-TBR-TTP model would achieve highest accuracy as it includes all available information, the AUC did not improve, which may be related to the limited value of TBR information in this context, but this should be re-evaluated in larger cohorts. Taken together, as previously shown for other entities, it seems beneficial not to narrow the view to the clinical information alone when constructing a predictive model but to include radiomic signatures in clinical prediction studies as well, as the combination of clinical and radiomic information seems to be of particular value with regard to survival risk prediction [45]. When considered on its own, an AUC of 0.74 still does not seem satisfactory, as further underscored by a positive predictive value for the identification of a short-term survivor of only 47.1% even for the best model (see Table 3). From a clinical point of view, the positive and negative predictive values are highly useful metrics in the context of decision-making as they give an estimate on the correctness of a prediction. In the clinical setting, it would be particularly beneficial to identify patients at risk for short-term survival in order to facilitate the selection of more aggressive treatments or earlier inclusion in experimental treatment studies, rather

than just standard treatment, to which approximately 30% of patients do not respond. However, also the identification of long-term survivors would be helpful in the clinical routine, as pseudoprogression can occur in one-third of the patients and may, when misinterpreted as tumor progression on MRI, lead to a premature cessation of an effective treatment. Of note, while the positive predictive value was extremely low in all models, the negative predictive value, reflecting the predictability of long-term survival, reached 84% in the best model. Therefore, even though the overall accuracies of our prediction models may not yet be satisfactory for the clinical use and the low positive predictive values impede the prediction of a short-term survivor, the high negative predictive value may be helpful for clinical decision-making. Our study supports that within a neuropathologically homogenous group of aggressive IDH-wildtype glioblastomas, especially the combination of different types of information (in this case clinical data and radiomic signature) can add value to a survival prediction model and consequently hints to the potential, which lies in the inclusion of even further image-based information. Indeed, one might speculate that the addition of conventional MRI data and in a next step more sophisticated MRI data such as perfusion or diffusion-weighted MRI may further increase the power of survival risk prediction of the combined clinical-TTP model [46], but such analyses require a standardized imaging protocol to assure comparability of MRI-based radiomic features. In other tumor entities as well, especially multiparametric imaging approaches have shown highly promising results for survival prediction, e.g., reaching an accuracy of up to 98% in a study on cervical cancer as compared to only 56–60% for prediction models using the standard clinical variables alone [47, 48]. Accordingly, dual PET imaging studies including other tracers than [^{18}F]FET in IDH-wildtype glioblastoma, such as TSPO-ligands which offer complementary information to the [^{18}F]FET uptake [49], are of high potential to further increase the power of survival prediction models, as exemplified by recent successful multi-tracer PET prediction approaches in other entities, such as prostate cancer [50].

Although the number of patients included in the current study is by far higher than in most previous [^{18}F]FET PET radiomics studies, a further increase in patient numbers may in future result in outperforming radiomics-only based approaches, as already shown in large-scale analyses for other medical settings [51]. According to the above-generated multivariate LR-based formulas, the known risk factors of high WHO grade, unmethylated MGMT promoter, TERTp mutation as well as higher patient age and lower KPS at diagnosis of IDH-wildtype glioblastoma were more likely associated with short-term survival [52–55]. However, gender has different correlations in different formulas, which

⊘ Springer

35

is inconsistent with the literature [53], although the weight of this parameter was low. This may likewise be due to the relatively low number of patients included in this study.

Whereas, in clinical routine, established dynamic [^{18}F]FET PET parameters such as the time–activity curve and/or the slope are usually only derived from representative subvolumes of interest within the tumor [7, 9, 56], in the current study every single voxel of the tumor was analyzed in order to generate whole-tumor TTP maps of dynamic [^{18}F]FET PET images. This comprehensive whole-tumor approach facilitated radiomic features extraction in dynamic image data and ensured to account for heterogeneity of uptake kinetics which has a major clinical impact when assessing brain tumors in dynamic [^{18}F]FET PET [57]. In this context, a relationship between tumor heterogeneity and the STS group could be found in the feature *ClusterProminence (CP)*. CP belongs to the *Gray Level Co-occurrence Matrix (GLCM)* and measures the skewness and asymmetry of the GLCM. A higher value implies more asymmetry while a lower value indicates a peak near the mean value and less variation around the mean. This correlation with the STS group indicates that a patient with a heterogeneous tumor in dynamic [^{18}F]FET PET images is more likely to be identified as high-risk patient for short-term survival. Another exemplary radiomic feature, which is associated with the STS group, is *Maximum 3D diameter, 3D shape feature*. The latter is defined as the largest pairwise Euclidean distance between tumor surface mesh vertices. This correlation, in simplified terms, indicates that patients belonging to the STS group have a tumor that shows large spread on PET. This finding is consistent with the literature—large tumor volumes on [^{18}F]FET PET were reported to be associated with poor overall survival in glioblastoma patients before radiation therapy with concomitant and adjuvant temozolomide [32, 33]. Details of other features are shown in the Supplementary information.

There are several limitations to this study. Only single-center data have been investigated, which led to the relatively small sample size and the lack of external validation. Yet, only single-center data have been chosen in this study since dynamic [^{18}F]FET PET is not always acquired routinely in other centers and pooling PET data with differences in time framing, image reconstruction algorithm, and scanner type may require prior implementation and validation of, e.g., feature harmonization procedures [58]. Moreover, it should be noted that almost all previous [^{18}F]FET PET radiomics studies have been performed with much smaller numbers of cases. The reliability of the reported scores was additionally evaluated using nested cross-validation [59] with five random splits in the outer loop, yielding a high AUC variability of 10% for the TTP model, 15% for the TBR model, and 11% for the clinical model (Supplementary material S4). Thereby, different radiomic signatures were obtained for each split of the outer loop since feature selection and model building are not robust when dealing with small sample sizes. Feature selection represents a challenge and has an impact on the performance of prediction models. Other feature selection methods comprise, e.g., filter methods such as minimum redundancy maximum relevance (MRMR) or ensemble methods, which provide a good balance between robust feature selection and model performance. Wrapper methods such as RFE have the advantage that feature dependencies can be modeled and that they interact with the classifier, while also bearing the risk of overfitting [60]. To enable standardized segmentation of tumor regions, only positive [^{18}F]FET PET images were included. Furthermore, MRI-based radiomics, as a more widely established and complementary tool, were not included in this study. Future studies may benefit from the combined use of multiparametric MRI data.

Conclusion

This study built and evaluated prediction models for survival combining both radiomic features extracted from static and dynamic [^{18}F]FET PET and clinical parameters. Specifically, the combination of clinical parameters with radiomics based on dynamic [^{18}F]FET PET data achieved a higher prognostic accuracy for the individualized assessment of short-term survival in patients with newly diagnosed IDH-wildtype glioblastoma in comparison to models using conventional clinical parameters only. Although the final accuracy remained moderate, the integration of dynamic [^{18}F]FET PET radiomic data into clinical prediction models may improve patient stratification beyond established prognostic markers. Future prospective radiomic studies using multimodal imaging data are needed to evaluate whether the integration of additional imaging parameters may further improve the prognostic performance and enhance the clinical interpretation of the study results.

Data availability The data that support the findings of this study are available on request from the corresponding author, ZL. The data are not publicly available due to the privacy of research participants.

Code availability The code that support the findings of this study are available from ZL and LK on reasonable request.

Declarations

Ethics approval Ethical approval of the retrospective data analysis was given by the institutional review board of the LMU (#606–16) in accordance with the ICH Guideline for Good Clinical Practice (GCP) and the declaration of Helsinki.

Consent to participate All patients have given written informed consent prior to the PET examination.

Conflict of interest The authors declare no competing interests.

References

1. Louis DN, Perry A, Reifenberger G, von Deimling A, Figarella-Branger D, Cavenee WK, et al. The 2016 World Health Organization Classification of Tumors of the Central Nervous System: a summary. Acta Neuropathol. 2016;131:803–20. https://doi.org/10.1007/s00401-016-1545-1.
2. Louis DN, Perry A, Wesseling P, Brat DJ, Cree IA, Figarella-Branger D, et al. The 2021 WHO Classification of Tumors of the Central Nervous System: a summary. Neuro Oncol. 2021;23:1231–51. https://doi.org/10.1093/neuonc/noab106.
3. Tan AC, Ashley DM, López GY, Malinzak M, Friedman HS, Khasraw M. Management of glioblastoma: state of the art and future directions. CA Cancer J Clin. 2020;70:299–312. https://doi.org/10.3322/caac.21613.
4. Esteller M, Garcia-Foncillas J, Andion E, Goodman SN, Hidalgo OF, Vanaclocha V, et al. Inactivation of the DNA-repair gene MGMT and the clinical response of gliomas to alkylating agents. N Engl J Med. 2000;343:1350–4. https://doi.org/10.1056/nejm200011093431901.
5. Van Meir EG, Hadjipanayis CG, Norden AD, Shu HK, Wen PY, Olson JJ. Exciting new advances in neuro-oncology: the avenue to a cure for malignant glioma. CA Cancer J Clin. 2010;60:166–93. https://doi.org/10.3322/caac.20069.
6. Pace A, Dirven L, Koekkoek JAF, Golla H, Fleming J, Rudà R, et al. European Association for Neuro-Oncology (EANO) guidelines for palliative care in adults with glioma. Lancet Oncol. 2017;18:e330–e40. https://doi.org/10.1016/s1470-2045(17)30345-5.
7. Jansen NL, Suchorska B, Wenter V, Schmid-Tannwald C, Todica A, Eigenbrod S, et al. Prognostic significance of dynamic 18F-FET PET in newly diagnosed astrocytic high-grade glioma. J Nucl Med. 2015;56:9–15. https://doi.org/10.2967/jnumed.114.144675.
8. Jansen NL, Suchorska B, Wenter V, Eigenbrod S, Schmid-Tannwald C, Zwergal A, et al. Dynamic 18F-FET PET in newly diagnosed astrocytic low-grade glioma identifies high-risk patients. J Nucl Med. 2014;55:198–203. https://doi.org/10.2967/jnumed.113.122333.
9. Pöpperl G, Kreth FW, Mehrkens JH, Herms J, Seelos K, Koch W, et al. FET PET for the evaluation of untreated gliomas: correlation of FET uptake and uptake kinetics with tumour grading. Eur J Nucl Med Mol Imaging. 2007;34:1933–42. https://doi.org/10.1007/s00259-007-0534-y.
10. Albert NL, Weller M, Suchorska B, Galldiks N, Soffietti R, Kim MM, et al. Response Assessment in Neuro-Oncology working group and European Association for Neuro-Oncology recommendations for the clinical use of PET imaging in gliomas. Neuro Oncol. 2016;18:1199–208. https://doi.org/10.1093/neuonc/now058.
11. Kunz M, Albert NL, Unterrainer M, la Fougere C, Egensperger R, Schuller U, et al. Dynamic 18F-FET PET is a powerful imaging biomarker in gadolinium-negative gliomas. Neuro Oncol. 2019;21:274–84. https://doi.org/10.1093/neuonc/noy098.
12. Bauer EK, Stoffels G, Blau T, Reifenberger G, Felsberg J, Werner JM, et al. Prediction of survival in patients with IDH-wildtype astrocytic gliomas using dynamic O-(2-[(18)F]-fluoroethyl)-L-tyrosine PET. Eur J Nucl Med Mol Imaging. 2020;47:1486–95. https://doi.org/10.1007/s00259-020-04695-0.
13. Lohmann P, Elahmadawy MA, Gutsche R, Werner JM, Bauer EK, Ceccon G, et al. FET PET radiomics for differentiating pseudoprogression from early tumor progression in glioma patients post-chemoradiation. Cancers (Basel). 2020;12. https://doi.org/10.3390/cancers12123835.
14. Li Z, Kaiser L, Holzgreve A, Ruf VC, Suchorska B, Wenter V, et al. Prediction of TERTp-mutation status in IDH-wildtype high-grade gliomas using pre-treatment dynamic [18F]FET PET radiomics. Eur J Nucl Med Mol Imaging. 2021. https://doi.org/10.1007/s00259-021-05526-6.
15. Stupp R, Hegi ME, Mason WP, van den Bent MJ, Taphoorn MJ, Janzer RC, et al. Effects of radiotherapy with concomitant and adjuvant temozolomide versus radiotherapy alone on survival in glioblastoma in a randomised phase III study: 5-year analysis of the EORTC-NCIC trial. Lancet Oncol. 2009;10:459–66. https://doi.org/10.1016/s1470-2045(09)70025-7.
16. Zhang X, Lu H, Tian Q, Feng N, Yin L, Xu X, et al. A radiomics nomogram based on multiparametric MRI might stratify glioblastoma patients according to survival. Eur Radiol. 2019;29:5528–38. https://doi.org/10.1007/s00330-019-06069-z.
17. Langen KJ, Bartenstein P, Boecker H, Brust P, Coenen HH, Drzezga A, et al. German guidelines for brain tumour imaging by PET and SPECT using labelled amino acids. Nuklearmedizin. 2011;50:167–73. https://doi.org/10.3413/nuk-2011041.
18. Unterrainer M, Vettermann F, Brendel M, Holzgreve A, Lifschitz M, Zahringer M, et al. Towards standardization of 18F-FET PET imaging: do we need a consistent method of background activity assessment? EJNMMI Res. 2017;7:48.
19. Law I, Albert NL, Arbizu J, Boellaard R, Drzezga A, Galldiks N, et al. Joint EANM/EANO/RANO practice guidelines/SNMMI procedure standards for imaging of gliomas using PET with radiolabelled amino acids and [(18)F]FDG: version 1.0. Eur J Nucl Med Mol Imaging. 2019;46:540–57. https://doi.org/10.1007/s00259-018-4207-9.

20. Pauleit D, Floeth F, Hamacher K, Riemenschneider MJ, Reifenberger G, Muller HW, et al. O-(2-[18F]fluoroethyl)-L-tyrosine PET combined with MRI improves the diagnostic assessment of cerebral gliomas. Brain. 2005;128:678–87. https://doi.org/10.1093/brain/awh399.

21. Vomacka L, Unterrainer M, Holzgreve A, Mille E, Gosewisch A, Brosch J, et al. Voxel-wise analysis of dynamic 18F-FET PET: a novel approach for non-invasive glioma characterisation. EJNMMI Res. 2018;8:91. https://doi.org/10.1186/s13550-018-0444-y.

22. Van Griethuysen JJM, Fedorov A, Parmar C, Hosny A, Aucoin N, Narayan V, et al. Computational radiomics system to decode the radiographic phenotype. Can Res. 2017;77:e104–7. https://doi.org/10.1158/0008-5472.can-17-0339.

23. Zwanenburg A, Vallières M, Abdalah MA, Aerts H, Andrearczyk V, Apte A, et al. The image biomarker standardization initiative: standardized quantitative radiomics for high-throughput image-based phenotyping. Radiology. 2020;295:328–38. https://doi.org/10.1148/radiol.2020191145.

24. Leijenaar RT, Nalbantov G, Carvalho S, van Elmpt WJ, Troost EG, Boellaard R, et al. The effect of SUV discretization in quantitative FDG-PET radiomics: the need for standardized methodology in tumor texture analysis. Sci Rep. 2015;5:11075. https://doi.org/10.1038/srep11075.

25. Kaiser LGM, Ahmadi SA, Unterrainer M, Holzgreve A, Mille E, Gosewisch A, Brosch J, Suchorska B, Navab N, Tonn JC, Ziegler S, Bartenstein P, Albert NL, Böning G. Annual Congress of the European Association of Nuclear Medicine October 12–16, 2019 Barcelona, Spain. Eur J Nucl Med Mol Imaging. 2019;46:1–952. https://doi.org/10.1007/s00259-019-04486-2.

26. Song Y, Zhang J, Zhang Y-D, Hou Y, Yan X, Wang Y, et al. FeAture Explorer (FAE): a tool for developing and comparing radiomics models. PLoS ONE. 2020;15:e0237587. https://doi.org/10.1371/journal.pone.0237587.

27. Pedregosa F, Varoquaux G, Gramfort A, Michel V, Thirion B, Grisel O, et al. Scikit-learn: machine learning in Python. J Mach Learn Res. 2011;12:2825–30.

28. Tomz M, King G, Zeng L. ReLogit: rare events logistic regression. 2003. 2003;8:27. https://doi.org/10.18637/jss.v008.i02.

29. Cohen I, Huang Y, Chen J, Benesty J. Noise reduction in speech processing. Springer topics in signal processing. Springer Berlin Heidelberg; 2009.

30. Chen C, Qin Y, Cheng J, Gao F, Zhou X. Texture analysis of fat-suppressed T2-weighted magnetic resonance imaging and use of machine learning to discriminate nasal and paranasal sinus small round malignant cell tumors. Front Oncol. 2021;11:701289. https://doi.org/10.3389/fonc.2021.701289.

31. Granitto PM, Furlanello C, Biasioli F, Gasperi F. Recursive feature elimination with random forest for PTR-MS analysis of agroindustrial products. Chemom Intell Lab Syst. 2006;83:83–90. https://doi.org/10.1016/j.chemolab.2006.01.007.

32. Suchorska B, Jansen NL, Linn J, Kretzschmar H, Janssen H, Eigenbrod S, et al. Biological tumor volume in 18FET-PET before radiochemotherapy correlates with survival in GBM. Neurology. 2015;84:710–9. https://doi.org/10.1212/wnl.0000000000001262.

33. Poulsen SH, Urup T, Grunnet K, Christensen IJ, Larsen VA, Jensen ML, et al. The prognostic value of FET PET at radiotherapy planning in newly diagnosed glioblastoma. Eur J Nucl Med Mol Imaging. 2017;44:373–81. https://doi.org/10.1007/s00259-016-3494-2.

34. Suchorska B, Giese A, Biczok A, Unterrainer M, Weller M, Drexler M, et al. Identification of time-to-peak on dynamic 18F-FET-PET as a prognostic marker specifically in IDH1/2 mutant diffuse astrocytoma. Neuro Oncol. 2018;20:279–88. https://doi.org/10.1093/neuonc/nox153.

35. Mittlmeier LM, Suchorska B, Ruf V, Holzgreve A, Brendel M, Herms J, et al. (18)F-FET PET Uptake characteristics of long-term IDH-wildtype diffuse glioma survivors. Cancers (Basel). 2021;13. https://doi.org/10.3390/cancers13133163.

36. Zhang X, Lu D, Gao P, Tian Q, Lu H, Xu X, et al. Survival-relevant high-risk subregion identification for glioblastoma patients: the MRI-based multiple instance learning approach. Eur Radiol. 2020;30:5602–10. https://doi.org/10.1007/s00330-020-06912-8.

37. Bae S, Choi YS, Ahn SS, Chang JH, Kang SG, Kim EH, et al. Radiomic MRI phenotyping of glioblastoma: improving survival prediction. Radiology. 2018;289:797–806. https://doi.org/10.1148/radiol.2018180200.

38. Liao X, Cai B, Tian B, Luo Y, Song W, Li Y. Machine-learning based radiogenomics analysis of MRI features and metagenes in glioblastoma multiforme patients with different survival time. J Cell Mol Med. 2019;23:4375–85. https://doi.org/10.1111/jcmm.14328.

39. Choi Y, Nam Y, Jang J, Shin NY, Lee YS, Ahn KJ, et al. Radiomics may increase the prognostic value for survival in glioblastoma patients when combined with conventional clinical and genetic prognostic models. Eur Radiol. 2021;31:2084–93. https://doi.org/10.1007/s00330-020-07335-1.

40. Xu Y, He X, Li Y, Pang P, Shu Z, Gong X. The nomogram of MRI-based radiomics with complementary visual features by machine learning improves stratification of glioblastoma patients: a multicenter study. J Magn Reson Imaging. 2021;54:571–83. https://doi.org/10.1002/jmri.27536.

41. Lohmann P, Kocher M, Ceccon G, Bauer EK, Stoffels G, Viswanathan S, et al. Combined FET PET/MRI radiomics differentiates radiation injury from recurrent brain metastasis. Neuroimage Clin. 2018;20:537–42. https://doi.org/10.1016/j.nicl.2018.08.024.

42. Carles M, Popp I, Starke MM, Mix M, Urbach H, Schimek-Jasch T, et al. FET-PET radiomics in recurrent glioblastoma: prognostic value for outcome after re-irradiation? Radiat Oncol (London, England). 2021;16:46. https://doi.org/10.1186/s13014-020-01744-8.

43. Paprottka KJ, Kleiner S, Preibisch C, Kofler F, Schmidt-Graf F, Delbridge C, et al. Fully automated analysis combining [(18)F]-FET-PET and multiparametric MRI including DSC perfusion and APTw imaging: a promising tool for objective evaluation of glioma progression. Eur J Nucl Med Mol Imaging. 2021;48:4445–55. https://doi.org/10.1007/s00259-021-05427-8.

44. Pencina MJ, D'Agostino RB Sr, D'Agostino RB Jr, Vasan RS. Evaluating the added predictive ability of a new marker: from area under the ROC curve to reclassification and beyond. Stat Med. 2008;27:157–72. https://doi.org/10.1002/sim.2929 (discussion 207-12).

45. Huang YQ, Liang CH, He L, Tian J, Liang CS, Chen X, et al. Development and validation of a radiomics nomogram for preoperative prediction of lymph node metastasis in colorectal cancer. J Clin Oncol. 2016;34:2157–64. https://doi.org/10.1200/jco.2015.65.9128.

46. Galldiks N, Zadeh G, Lohmann P. Artificial intelligence, radiomics, and deep learning in neuro-oncology. Neurooncol Adv. 2020;2:iv1–2. https://doi.org/10.1093/noajnl/vdaa179.

47. Lucia F, Visvikis D, Desseroit MC, Miranda O, Malhaire JP, Robin P, et al. Prediction of outcome using pretreatment (18)F-FDG PET/CT and MRI radiomics in locally advanced cervical cancer treated with chemoradiotherapy. Eur J Nucl Med Mol Imaging. 2018;45:768–86. https://doi.org/10.1007/s00259-017-3898-7.

48. Lucia F, Visvikis D, Vallières M, Desseroit MC, Miranda O, Robin P, et al. External validation of a combined PET and MRI radiomics model for prediction of recurrence in cervical cancer patients treated with chemoradiotherapy. Eur J Nucl Med Mol Imaging. 2019;46:864–77. https://doi.org/10.1007/s00259-018-4231-9.

49. Unterrainer M, Fleischmann DF, Diekmann C, Vomacka L, Lindner S, Vettermann F, et al. Comparison of (18)F-GE-180 and dynamic (18)F-FET PET in high grade glioma: a double-tracer pilot study. Eur J Nucl Med Mol Imaging. 2019;46:580–90. https://doi.org/10.1007/s00259-018-4166-1.

50. Michalski K, Ruf J, Goetz C, Seitz AK, Buck AK, Lapa C, et al. Prognostic implications of dual tracer PET/CT: PSMA ligand and [(18)F]FDG PET/CT in patients undergoing [(177)Lu]PSMA radioligand therapy. Eur J Nucl Med Mol Imaging. 2021;48:2024–30. https://doi.org/10.1007/s00259-020-05160-8.

51. Esteva A, Kuprel B, Novoa RA, Ko J, Swetter SM, Blau HM, et al. Dermatologist-level classification of skin cancer with deep neural networks. Nature. 2017;542:115–8. https://doi.org/10.1038/nature21056.

52. Reifenberger G, Weber RG, Riehmer V, Kaulich K, Willscher E, Wirth H, et al. Molecular characterization of long-term survivors of glioblastoma using genome-and transcriptome-wide profiling. Int J Cancer. 2014;135:1822–31.

53. Burgenske DM, Yang J, Decker PA, Kollmeyer TM, Kosel ML, Mladek AC, et al. Molecular profiling of long-term IDH-wildtype glioblastoma survivors. Neuro Oncol. 2019;21:1458–69.

54. Park JK, Hodges T, Arko L, Shen M, Iacono DD, McNabb A, et al. Scale to predict survival after surgery for recurrent glioblastoma multiforme. J Clin Oncol. 2010;28:3838.

55. Simon M, Hosen I, Gousias K, Rachakonda S, Heidenreich B, Gessi M, et al. TERT promoter mutations: a novel independent prognostic factor in primary glioblastomas. Neuro Oncol. 2015;17:45–52. https://doi.org/10.1093/neuonc/nou158.

56. Jansen NL, Graute V, Armbruster L, Suchorska B, Lutz J, Eigenbrod S, et al. MRI-suspected low-grade glioma: is there a need to perform dynamic FET PET? Eur J Nucl Med Mol Imaging. 2012;39:1021–9. https://doi.org/10.1007/s00259-012-2109-9.

57. Kunz M, Thon N, Eigenbrod S, Hartmann C, Egensperger R, Herms J, et al. Hot spots in dynamic (18)FET-PET delineate malignant tumor parts within suspected WHO grade II gliomas. Neuro Oncol. 2011;13:307–16. https://doi.org/10.1093/neuonc/noq196.

58. Da-Ano R, Masson I, Lucia F, Doré M, Robin P, Alfieri J, et al. Performance comparison of modified ComBat for harmonization of radiomic features for multicenter studies. Sci Rep. 2020;10:10248. https://doi.org/10.1038/s41598-020-66110-w.

59. Varma S, Simon R. Bias in error estimation when using cross-validation for model selection. BMC Bioinformatics. 2006;7:91. https://doi.org/10.1186/1471-2105-7-91.

60. Saeys Y, Inza I, Larranaga P. A review of feature selection techniques in bioinformatics. Bioinformatics. 2007;23:2507–17. https://doi.org/10.1093/bioinformatics/btm344.

Authors and Affiliations

Zhicong Li[1] ⬤ · **Adrien Holzgreve**[1] · **Lena M. Unterrainer**[1] · **Viktoria C. Ruf**[2] · **Stefanie Quach**[3] · **Laura M. Bartos**[1] · **Bogdana Suchorska**[3,4] · **Maximilian Niyazi**[5,6] · **Vera Wenter**[1] · **Jochen Herms**[2] · **Peter Bartenstein**[1,6] · **Joerg-Christian Tonn**[3,6] · **Marcus Unterrainer**[7] · **Nathalie L. Albert**[1,6] · **Lena Kaiser**[1]

[1] Department of Nuclear Medicine, University Hospital, LMU Munich, Marchioninistr. 15, 81377 Munich, Germany

[2] Center for Neuropathology and Prion Research, LMU Munich, Munich, Germany

[3] Department of Neurosurgery, University Hospital, LMU Munich, Munich, Germany

[4] Department of Neurosurgery, Sana Hospital, Duisburg, Germany

[5] Department of Radiotherapy, University Hospital, LMU Munich, Munich, Germany

[6] German Cancer Consortium (DKTK), Partner Site Munich, German Cancer Research Center (DKFZ), Heidelberg, Germany

[7] Department of Radiology, University Hospital, LMU Munich, Munich, Germany

⌖ Springer

References

Albert, N. L., Winkelmann, I., Suchorska, B., Wenter, V., Schmid-Tannwald, C., Mille, E., . . . la Fougère, C. (2016). Early static (18)F-FET-PET scans have a higher accuracy for glioma grading than the standard 20-40 min scans. *Eur J Nucl Med Mol Imaging, 43*(6), 1105-1114. doi:10.1007/s00259-015-3276-2

Albert, N. L., Winkelmann, I., Suchorska, B., Wenter, V., Schmid-Tannwald, C., Mille, E., . . . la Fougere, C. (2016). Early static (18)F-FET-PET scans have a higher accuracy for glioma grading than the standard 20-40 min scans. *Eur J Nucl Med Mol Imaging, 43*(6), 1105-1114. doi:10.1007/s00259-015-3276-2

Arita, H., Narita, Y., Takami, H., Fukushima, S., Matsushita, Y., Yoshida, A., . . . Ichimura, K. (2013). TERT promoter mutations rather than methylation are the main mechanism for TERT upregulation in adult gliomas. *Acta Neuropathol, 126*(6), 939-941. doi:10.1007/s00401-013-1203-9

Bagherzadeh-Khiabani, F., Ramezankhani, A., Azizi, F., Hadaegh, F., Steyerberg, E. W., & Khalili, D. (2016). A tutorial on variable selection for clinical prediction models: feature selection methods in data mining could improve the results. *J Clin Epidemiol, 71*, 76-85. doi:10.1016/j.jclinepi.2015.10.002

Barthel, F. P., Wei, W., Tang, M., Martinez-Ledesma, E., Hu, X., Amin, S. B., . . . Verhaak, R. G. (2017). Systematic analysis of telomere length and somatic alterations in 31 cancer types. *Nat Genet, 49*(3), 349-357. doi:10.1038/ng.3781

Batista, R., Cruvinel-Carloni, A., Vinagre, J., Peixoto, J., Catarino, T. A., Campanella, N. C., . . . Lima, J. (2016). The prognostic impact of TERT promoter mutations in glioblastomas is modified by the rs2853669 single nucleotide polymorphism. *Int J Cancer, 139*(2), 414-423. doi:10.1002/ijc.30057

Bodnar, A. G., Ouellette, M., Frolkis, M., Holt, S. E., Chiu, C. P., Morin, G. B., . . . Wright, W. E. (1998). Extension of life-span by introduction of telomerase into normal human cells. *Science, 279*(5349), 349-352. doi:10.1126/science.279.5349.349

Brandsma, D., Stalpers, L., Taal, W., Sminia, P., & van den Bent, M. J. (2008). Clinical features, mechanisms, and management of pseudoprogression in malignant gliomas. *Lancet Oncol, 9*(5), 453-461. doi:10.1016/s1470-2045(08)70125-6

Brandsma, D., & van den Bent, M. J. (2009). Pseudoprogression and pseudoresponse in the treatment of gliomas. *Curr Opin Neurol, 22*(6), 633-638. doi:10.1097/WCO.0b013e328332363e

Brat, D. J., Aldape, K., Colman, H., Holland, E. C., Louis, D. N., Jenkins, R. B., . . . Weller, M. (2018). cIMPACT-NOW update 3: recommended diagnostic criteria for "Diffuse astrocytic glioma, IDH-wildtype, with molecular features of glioblastoma, WHO grade IV". *Acta Neuropathol, 136*(5), 805-810. doi:10.1007/s00401-018-1913-0

Calcagni, M. L., Galli, G., Giordano, A., Taralli, S., Anile, C., Niesen, A., & Baum, R. P. (2011). Dynamic O-(2-[18F]fluoroethyl)-L-tyrosine (F-18 FET) PET for glioma grading: assessment of individual probability of malignancy. *Clin Nucl Med, 36*(10), 841-847. doi:10.1097/RLU.0b013e3182291b40

Carles, M., Popp, I., Starke, M. M., Mix, M., Urbach, H., Schimek-Jasch, T., . . . Grosu, A. L. (2021). FET-PET radiomics in recurrent glioblastoma: prognostic value for outcome after re-irradiation? *Radiat Oncol, 16*(1), 46. doi:10.1186/s13014-020-01744-8

Ceccon, G., Lohmann, P., Stoffels, G., Judov, N., Filss, C. P., Rapp, M., . . . Galldiks, N. (2017). Dynamic O-(2-18F-fluoroethyl)-L-tyrosine positron emission tomography differentiates brain metastasis recurrence from radiation injury after radiotherapy. *Neuro Oncol, 19*(2), 281-288. doi:10.1093/neuonc/now149

de Lange, T. (2009). How telomeres solve the end-protection problem. *Science, 326*(5955), 948-952. doi:10.1126/science.1170633

Dunet, V., Rossier, C., Buck, A., Stupp, R., & Prior, J. O. (2012). Performance of 18F-fluoro-ethyl-tyrosine (18F-FET) PET for the differential diagnosis of primary brain tumor: a systematic review and Metaanalysis. *J Nucl Med, 53*(2), 207-214. doi:10.2967/jnumed.111.096859

Eckel-Passow, J. E., Lachance, D. H., Molinaro, A. M., Walsh, K. M., Decker, P. A., Sicotte, H., . . . Jenkins, R. B. (2015). Glioma Groups Based on 1p/19q, IDH, and TERT Promoter Mutations in Tumors. *N Engl J Med, 372*(26), 2499-2508. doi:10.1056/NEJMoa1407279

Esteller, M., Garcia-Foncillas, J., Andion, E., Goodman, S. N., Hidalgo, O. F., Vanaclocha, V., . . . Herman, J. G. (2000). Inactivation of the DNA-repair gene MGMT and the clinical response of gliomas to alkylating agents. *N Engl J Med, 343*(19), 1350-1354. doi:10.1056/nejm200011093431901

Fang, S., Fan, Z., Sun, Z., Li, Y., Liu, X., Liang, Y., . . . Wang, L. (2020). Radiomics Features Predict Telomerase Reverse Transcriptase Promoter Mutations in World Health Organization Grade II Gliomas via a Machine-Learning Approach. *Front Oncol, 10*, 606741. doi:10.3389/fonc.2020.606741

Floeth, F. W., Pauleit, D., Sabel, M., Stoffels, G., Reifenberger, G., Riemenschneider, M. J., . . . Langen, K. J. (2007). Prognostic value of O-(2-18F-fluoroethyl)-L-tyrosine PET and MRI in low-grade glioma. *J Nucl Med, 48*(4), 519-527. doi:10.2967/jnumed.106.037895

Galavis, P. E., Hollensen, C., Jallow, N., Paliwal, B., & Jeraj, R. (2010). Variability of textural features in FDG PET images due to different acquisition modes and reconstruction parameters. *Acta Oncol, 49*(7), 1012-1016. doi:10.3109/0284186x.2010.498437

Galldiks, N., Dunkl, V., Stoffels, G., Hutterer, M., Rapp, M., Sabel, M., . . . Langen, K. J. (2015). Diagnosis of pseudoprogression in patients with glioblastoma using O-(2-[18F]fluoroethyl)-L-tyrosine PET. *Eur J Nucl Med Mol Imaging, 42*(5), 685-695. doi:10.1007/s00259-014-2959-4

Galldiks, N., Langen, K. J., Holy, R., Pinkawa, M., Stoffels, G., Nolte, K. W., . . . Piroth, M. D. (2012). Assessment of treatment response in patients with glioblastoma using O-(2-18F-fluoroethyl)-L-tyrosine PET in comparison to MRI. *J Nucl Med, 53*(7), 1048-1057. doi:10.2967/jnumed.111.098590

Galldiks, N., Langen, K. J., & Pope, W. B. (2015). From the clinician's point of view - What is the status quo of positron emission tomography in patients with brain tumors? *Neuro Oncol, 17*(11), 1434-1444. doi:10.1093/neuonc/nov118

Galldiks, N., Rapp, M., Stoffels, G., Fink, G. R., Shah, N. J., Coenen, H. H., . . . Langen, K. J. (2013). Response assessment of bevacizumab in patients with recurrent malignant glioma using [18F]Fluoroethyl-L-tyrosine PET in comparison to MRI. *Eur J Nucl Med Mol Imaging, 40*(1), 22-33. doi:10.1007/s00259-012-2251-4

Galldiks, N., Stoffels, G., Filss, C., Rapp, M., Blau, T., Tscherpel, C., . . . Langen, K. J. (2015). The use of dynamic O-(2-18F-fluoroethyl)-l-tyrosine PET in the diagnosis of patients with progressive and recurrent glioma. *Neuro Oncol, 17*(9), 1293-1300. doi:10.1093/neuonc/nov088

Gillies, R. J., Kinahan, P. E., & Hricak, H. (2016). Radiomics: Images Are More than Pictures, They Are Data. *Radiology, 278*(2), 563-577. doi:10.1148/radiol.2015151169

Greider, C. W., & Blackburn, E. H. (1985). Identification of a specific telomere terminal transferase activity in Tetrahymena extracts. *Cell, 43*(2 Pt 1), 405-413. doi:10.1016/0092-8674(85)90170-9

Grootjans, W., Tixier, F., van der Vos, C. S., Vriens, D., Le Rest, C. C., Bussink, J., . . . Visser, E. P. (2016). The Impact of Optimal Respiratory Gating and Image Noise on Evaluation of Intratumor Heterogeneity on 18F-FDG PET Imaging of Lung Cancer. *J Nucl Med, 57*(11), 1692-1698. doi:10.2967/jnumed.116.173112

Hanahan, D., & Weinberg, R. A. (2011). Hallmarks of cancer: the next generation. *Cell, 144*(5), 646-674. doi:10.1016/j.cell.2011.02.013

Haubold, J., Demircioglu, A., Gratz, M., Glas, M., Wrede, K., Sure, U., . . . Umutlu, L. (2020). Non-invasive tumor decoding and phenotyping of cerebral gliomas utilizing multiparametric (18)F-FET PET-MRI and MR Fingerprinting. *Eur J Nucl Med Mol Imaging, 47*(6), 1435-1445. doi:10.1007/s00259-019-04602-2

Heidenreich, B., Nagore, E., Rachakonda, P. S., Garcia-Casado, Z., Requena, C., Traves, V., . . . Kumar, R. (2014). Telomerase reverse transcriptase promoter mutations in primary cutaneous melanoma. *Nat Commun, 5*, 3401. doi:10.1038/ncomms4401

Hockemeyer, D., & Collins, K. (2015). Control of telomerase action at human telomeres. *Nat Struct Mol Biol, 22*(11), 848-852. doi:10.1038/nsmb.3083

Holt, S. E., Wright, W. E., & Shay, J. W. (1996). Regulation of telomerase activity in immortal cell lines. *Mol Cell Biol, 16*(6), 2932-2939. doi:10.1128/mcb.16.6.2932

Huang, D. S., Wang, Z., He, X. J., Diplas, B. H., Yang, R., Killela, P. J., . . . Tao, H. Q. (2015). Recurrent TERT promoter mutations identified in a large-scale study of multiple tumour types are associated with increased TERT expression and telomerase activation. *Eur J Cancer, 51*(8), 969-976. doi:10.1016/j.ejca.2015.03.010

Hutterer, M., Nowosielski, M., Putzer, D., Jansen, N. L., Seiz, M., Schocke, M., . . . Stockhammer, G. (2013). [18F]-fluoro-ethyl-L-tyrosine PET: a valuable diagnostic tool in neuro-oncology, but not all that glitters is glioma. *Neuro Oncol, 15*(3), 341-351. doi:10.1093/neuonc/nos300

Hutterer, M., Nowosielski, M., Putzer, D., Waitz, D., Tinkhauser, G., Kostron, H., . . . Stockhammer, G. (2011). O-(2-18F-fluoroethyl)-L-tyrosine PET predicts failure of antiangiogenic

treatment in patients with recurrent high-grade glioma. *J Nucl Med, 52*(6), 856-864. doi:10.2967/jnumed.110.086645

Jansen, N. L., Graute, V., Armbruster, L., Suchorska, B., Lutz, J., Eigenbrod, S., . . . la Fougere, C. (2012). MRI-suspected low-grade glioma: is there a need to perform dynamic FET PET? *Eur J Nucl Med Mol Imaging, 39*(6), 1021-1029. doi:10.1007/s00259-012-2109-9

Jansen, N. L., Suchorska, B., Wenter, V., Eigenbrod, S., Schmid-Tannwald, C., Zwergal, A., . . . la Fougère, C. (2014). Dynamic 18F-FET PET in newly diagnosed astrocytic low-grade glioma identifies high-risk patients. *J Nucl Med, 55*(2), 198-203. doi:10.2967/jnumed.113.122333

Jansen, N. L., Suchorska, B., Wenter, V., Eigenbrod, S., Schmid-Tannwald, C., Zwergal, A., . . . la Fougere, C. (2014). Dynamic 18F-FET PET in newly diagnosed astrocytic low-grade glioma identifies high-risk patients. *J Nucl Med, 55*(2), 198-203. doi:10.2967/jnumed.113.122333

Jansen, N. L., Suchorska, B., Wenter, V., Schmid-Tannwald, C., Todica, A., Eigenbrod, S., . . . la Fougère, C. (2015). Prognostic significance of dynamic 18F-FET PET in newly diagnosed astrocytic high-grade glioma. *J Nucl Med, 56*(1), 9-15. doi:10.2967/jnumed.114.144675

Jansen, N. L., Suchorska, B., Wenter, V., Schmid-Tannwald, C., Todica, A., Eigenbrod, S., . . . la Fougere, C. (2015). Prognostic significance of dynamic 18F-FET PET in newly diagnosed astrocytic high-grade glioma. *J Nucl Med, 56*(1), 9-15. doi:10.2967/jnumed.114.144675

Jiang, C., Kong, Z., Zhang, Y., Liu, S., Liu, Z., Chen, W., . . . Ma, W. (2020). Conventional magnetic resonance imaging-based radiomic signature predicts telomerase reverse transcriptase promoter mutation status in grade II and III gliomas. *Neuroradiology, 62*(7), 803-813. doi:10.1007/s00234-020-02392-1

Kebir, S., Fimmers, R., Galldiks, N., Schäfer, N., Mack, F., Schaub, C., . . . Herrlinger, U. (2016). Late Pseudoprogression in Glioblastoma: Diagnostic Value of Dynamic O-(2-[18F]fluoroethyl)-L-Tyrosine PET. *Clin Cancer Res, 22*(9), 2190-2196. doi:10.1158/1078-0432.Ccr-15-1334

Kickingereder, P., Götz, M., Muschelli, J., Wick, A., Neuberger, U., Shinohara, R. T., . . . Bonekamp, D. (2016). Large-scale Radiomic Profiling of Recurrent Glioblastoma Identifies an Imaging Predictor for Stratifying Anti-Angiogenic Treatment Response. *Clin Cancer Res, 22*(23), 5765-5771. doi:10.1158/1078-0432.Ccr-16-0702

Killela, P. J., Reitman, Z. J., Jiao, Y., Bettegowda, C., Agrawal, N., Diaz, L. A., Jr., . . . Yan, H. (2013). TERT promoter mutations occur frequently in gliomas and a subset of tumors derived from cells with low rates of self-renewal. *Proc Natl Acad Sci U S A, 110*(15), 6021-6026. doi:10.1073/pnas.1303607110

Kim, J. Y., Park, J. E., Jo, Y., Shim, W. H., Nam, S. J., Kim, J. H., . . . Kim, H. S. (2019). Incorporating diffusion- and perfusion-weighted MRI into a radiomics model improves diagnostic performance for pseudoprogression in glioblastoma patients. *Neuro Oncol, 21*(3), 404-414. doi:10.1093/neuonc/noy133

Kratochwil, C., Combs, S. E., Leotta, K., Afshar-Oromieh, A., Rieken, S., Debus, J., . . . Giesel, F. L. (2014). Intra-individual comparison of ^{18}F-FET and ^{18}F-DOPA in PET imaging of recurrent brain tumors. *Neuro Oncol, 16*(3), 434-440. doi:10.1093/neuonc/not199

Kumar, V., Gu, Y., Basu, S., Berglund, A., Eschrich, S. A., Schabath, M. B., . . . Gillies, R. J. (2012). Radiomics: the process and the challenges. *Magn Reson Imaging, 30*(9), 1234-1248. doi:10.1016/j.mri.2012.06.010

Kunz, M., Albert, N. L., Unterrainer, M., la Fougere, C., Egensperger, R., Schüller, U., . . . Thon, N. (2019). Dynamic 18F-FET PET is a powerful imaging biomarker in gadolinium-negative gliomas. *Neuro Oncol, 21*(2), 274-284. doi:10.1093/neuonc/noy098

Kunz, M., Thon, N., Eigenbrod, S., Hartmann, C., Egensperger, R., Herms, J., . . . Kreth, F. W. (2011). Hot spots in dynamic (18)FET-PET delineate malignant tumor parts within suspected WHO grade II gliomas. *Neuro Oncol, 13*(3), 307-316. doi:10.1093/neuonc/noq196

Labussière, M., Di Stefano, A. L., Gleize, V., Boisselier, B., Giry, M., Mangesius, S., . . . Sanson, M. (2014). TERT promoter mutations in gliomas, genetic associations and clinico-pathological correlations. *Br J Cancer, 111*(10), 2024-2032. doi:10.1038/bjc.2014.538

Lambin, P., Rios-Velazquez, E., Leijenaar, R., Carvalho, S., van Stiphout, R. G., Granton, P., . . . Aerts, H. J. (2012). Radiomics: extracting more information from medical images using advanced feature analysis. *Eur J Cancer, 48*(4), 441-446. doi:10.1016/j.ejca.2011.11.036

Langen, K. J., Bartenstein, P., Boecker, H., Brust, P., Coenen, H. H., Drzezga, A., . . . Schreckenberger, M. (2011). [German guidelines for brain tumour imaging by PET and SPECT using labelled amino acids]. *Nuklearmedizin, 50*(4), 167-173. doi:10.3413/nuk-

2011041

Larue, R. T., Defraene, G., De Ruysscher, D., Lambin, P., & van Elmpt, W. (2017). Quantitative radiomics studies for tissue characterization: a review of technology and methodological procedures. *Br J Radiol, 90*(1070), 20160665. doi:10.1259/bjr.20160665

Leão, R., Apolónio, J. D., Lee, D., Figueiredo, A., Tabori, U., & Castelo-Branco, P. (2018). Mechanisms of human telomerase reverse transcriptase (hTERT) regulation: clinical impacts in cancer. *J Biomed Sci, 25*(1), 22. doi:10.1186/s12929-018-0422-8

Li, Y., Ammari, S., Lawrance, L., Quillent, A., Assi, T., Lassau, N., & Chouzenoux, E. (2022). Radiomics-Based Method for Predicting the Glioma Subtype as Defined by Tumor Grade, IDH Mutation, and 1p/19q Codeletion. *Cancers (Basel), 14*(7). doi:10.3390/cancers14071778

Li, Y., Liu, X., Qian, Z., Sun, Z., Xu, K., Wang, K., . . . Jiang, T. (2018). Genotype prediction of ATRX mutation in lower-grade gliomas using an MRI radiomics signature. *Eur Radiol, 28*(7), 2960-2968. doi:10.1007/s00330-017-5267-0

Li, Y., Liu, X., Xu, K., Qian, Z., Wang, K., Fan, X., . . . Jiang, T. (2018). MRI features can predict EGFR expression in lower grade gliomas: A voxel-based radiomic analysis. *Eur Radiol, 28*(1), 356-362. doi:10.1007/s00330-017-4964-z

Li, Y., Qian, Z., Xu, K., Wang, K., Fan, X., Li, S., . . . Wang, Y. (2018). MRI features predict p53 status in lower-grade gliomas via a machine-learning approach. *Neuroimage Clin, 17*, 306-311. doi:10.1016/j.nicl.2017.10.030

Li, Y., Qian, Z., Xu, K., Wang, K., Fan, X., Li, S., . . . Jiang, T. (2017). Radiomic features predict Ki-67 expression level and survival in lower grade gliomas. *J Neurooncol, 135*(2), 317-324. doi:10.1007/s11060-017-2576-8

Li, Z., Li, H., Wang, S., Dong, D., Yin, F., Chen, A., . . . Wang, H. (2019). MR-Based Radiomics Nomogram of Cervical Cancer in Prediction of the Lymph-Vascular Space Invasion preoperatively. *J Magn Reson Imaging, 49*(5), 1420-1426. doi:10.1002/jmri.26531

Li, Z., Zhang, J., Song, Y., Yin, X., Chen, A., Tang, N., . . . Wang, H. (2021). Utilization of radiomics to predict long-term outcome of magnetic resonance-guided focused ultrasound ablation therapy in adenomyosis. *Eur Radiol, 31*(1), 392-402. doi:10.1007/s00330-020-07076-1

Liu, L., Lai, S., Andrews, L. G., & Tollefsbol, T. O. (2004). Genetic and epigenetic modulation of telomerase activity in development and disease. *Gene, 340*(1), 1-10. doi:10.1016/j.gene.2004.06.011

Liu, Z., Wang, S., Dong, D., Wei, J., Fang, C., Zhou, X., . . . Tian, J. (2019). The Applications of Radiomics in Precision Diagnosis and Treatment of Oncology: Opportunities and Challenges. *Theranostics, 9*(5), 1303-1322. doi:10.7150/thno.30309

Lohmann, P., Elahmadawy, M. A., Gutsche, R., Werner, J. M., Bauer, E. K., Ceccon, G., . . . Galldiks, N. (2020). FET PET Radiomics for Differentiating Pseudoprogression from Early Tumor Progression in Glioma Patients Post-Chemoradiation. *Cancers (Basel), 12*(12). doi:10.3390/cancers12123835

Lohmann, P., Stoffels, G., Ceccon, G., Rapp, M., Sabel, M., Filss, C. P., . . . Galldiks, N. (2017). Radiation injury vs. recurrent brain metastasis: combining textural feature radiomics analysis and standard parameters may increase (18)F-FET PET accuracy without dynamic scans. *Eur Radiol, 27*(7), 2916-2927. doi:10.1007/s00330-016-4638-2

Louis, D. N., Perry, A., Reifenberger, G., von Deimling, A., Figarella-Branger, D., Cavenee, W. K., . . . Ellison, D. W. (2016). The 2016 World Health Organization Classification of Tumors of the Central Nervous System: a summary. *Acta Neuropathol, 131*(6), 803-820. doi:10.1007/s00401-016-1545-1

Louis, D. N., Perry, A., Wesseling, P., Brat, D. J., Cree, I. A., Figarella-Branger, D., . . . Ellison, D. W. (2021). The 2021 WHO Classification of Tumors of the Central Nervous System: a summary. *Neuro Oncol, 23*(8), 1231-1251. doi:10.1093/neuonc/noab106

Louis, D. N., Wesseling, P., Aldape, K., Brat, D. J., Capper, D., Cree, I. A., . . . Ellison, D. W. (2020). cIMPACT-NOW update 6: new entity and diagnostic principle recommendations of the cIMPACT-Utrecht meeting on future CNS tumor classification and grading. *Brain Pathol, 30*(4), 844-856. doi:10.1111/bpa.12832

Maciejowski, J., & de Lange, T. (2017). Telomeres in cancer: tumour suppression and genome instability. *Nat Rev Mol Cell Biol, 18*(3), 175-186. doi:10.1038/nrm.2016.171

Masutomi, K., Kaneko, S., Hayashi, N., Yamashita, T., Shirota, Y., Kobayashi, K., & Murakami, S. (2000). Telomerase activity reconstituted in vitro with purified human telomerase reverse transcriptase and human telomerase RNA component. *J Biol Chem, 275*(29), 22568-22573. doi:10.1074/jbc.M000622200

Nandakumar, J., & Cech, T. R. (2013). Finding the end: recruitment of telomerase to telomeres.

Nat Rev Mol Cell Biol, 14(2), 69-82. doi:10.1038/nrm3505

O'Sullivan, R. J., & Karlseder, J. (2010). Telomeres: protecting chromosomes against genome instability. *Nat Rev Mol Cell Biol, 11*(3), 171-181. doi:10.1038/nrm2848

Oliver, J. A., Budzevich, M., Zhang, G. G., Dilling, T. J., Latifi, K., & Moros, E. G. (2015). Variability of Image Features Computed from Conventional and Respiratory-Gated PET/CT Images of Lung Cancer. *Transl Oncol, 8*(6), 524-534. doi:10.1016/j.tranon.2015.11.013

Ostrom, Q. T., Cote, D. J., Ascha, M., Kruchko, C., & Barnholtz-Sloan, J. S. (2018). Adult Glioma Incidence and Survival by Race or Ethnicity in the United States From 2000 to 2014. *JAMA Oncol, 4*(9), 1254-1262. doi:10.1001/jamaoncol.2018.1789

Ostrom, Q. T., Gittleman, H., Truitt, G., Boscia, A., Kruchko, C., & Barnholtz-Sloan, J. S. (2018). CBTRUS Statistical Report: Primary Brain and Other Central Nervous System Tumors Diagnosed in the United States in 2011-2015. *Neuro Oncol, 20*(suppl_4), iv1-iv86. doi:10.1093/neuonc/noy131

Pace, A., Dirven, L., Koekkoek, J. A. F., Golla, H., Fleming, J., Rudà, R., . . . Taphoorn, M. J. B. European Association for Neuro-Oncology (EANO) guidelines for palliative care in adults with glioma. (1474-5488 (Electronic)).

Park, C. J., Han, K., Kim, H., Ahn, S. S., Choi, D., Park, Y. W., . . . Lee, S. K. (2021). MRI Features May Predict Molecular Features of Glioblastoma in Isocitrate Dehydrogenase Wild-Type Lower-Grade Gliomas. *AJNR Am J Neuroradiol, 42*(3), 448-456. doi:10.3174/ajnr.A6983

Pauleit, D., Floeth, F., Hamacher, K., Riemenschneider, M. J., Reifenberger, G., Müller, H. W., . . . Langen, K. J. (2005). O-(2-[18F]fluoroethyl)-L-tyrosine PET combined with MRI improves the diagnostic assessment of cerebral gliomas. *Brain, 128*(Pt 3), 678-687. doi:10.1093/brain/awh399

Peng, Y., Mian, I. S., & Lue, N. F. (2001). Analysis of telomerase processivity: mechanistic similarity to HIV-1 reverse transcriptase and role in telomere maintenance. *Mol Cell, 7*(6), 1201-1211. doi:10.1016/s1097-2765(01)00268-4

Piroth, M. D., Pinkawa, M., Holy, R., Klotz, J., Nussen, S., Stoffels, G., . . . Eble, M. J. (2011). Prognostic value of early [18F]fluoroethyltyrosine positron emission tomography after radiochemotherapy in glioblastoma multiforme. *Int J Radiat Oncol Biol Phys, 80*(1), 176-184. doi:10.1016/j.ijrobp.2010.01.055

Popperl, G., Kreth, F. W., Mehrkens, J. H., Herms, J., Seelos, K., Koch, W., . . . Tatsch, K. (2007). FET PET for the evaluation of untreated gliomas: correlation of FET uptake and uptake kinetics with tumour grading. *Eur J Nucl Med Mol Imaging, 34*(12), 1933-1942. doi:10.1007/s00259-007-0534-y

Pöpperl, G., Kreth, F. W., Mehrkens, J. H., Herms, J., Seelos, K., Koch, W., . . . Tatsch, K. (2007). FET PET for the evaluation of untreated gliomas: correlation of FET uptake and uptake kinetics with tumour grading. *Eur J Nucl Med Mol Imaging, 34*(12), 1933-1942. doi:10.1007/s00259-007-0534-y

Pyka, T., Hiob, D., Preibisch, C., Gempt, J., Wiestler, B., Schlegel, J., . . . Zimmer, C. (2018). Diagnosis of glioma recurrence using multiparametric dynamic 18F-fluoroethyl-tyrosine PET-MRI. *Eur J Radiol, 103*, 32-37. doi:10.1016/j.ejrad.2018.04.003

Rachakonda, S., Hoheisel, J. D., & Kumar, R. (2021). Occurrence, functionality and abundance of the TERT promoter mutations. *Int J Cancer, 149*(11), 1852-1862. doi:10.1002/ijc.33750

Rachinger, W., Goetz, C., Pöpperl, G., Gildehaus, F. J., Kreth, F. W., Holtmannspötter, M., . . . Tonn, J. C. (2005). Positron emission tomography with O-(2-[18F]fluoroethyl)-l-tyrosine versus magnetic resonance imaging in the diagnosis of recurrent gliomas. *Neurosurgery, 57*(3), 505-511; discussion 505-511. doi:10.1227/01.neu.0000171642.49553.b0

Roake, C. M., & Artandi, S. E. (2020). Regulation of human telomerase in homeostasis and disease. *Nat Rev Mol Cell Biol, 21*(7), 384-397. doi:10.1038/s41580-020-0234-z

Rushing, E. J. (2021). WHO classification of tumors of the nervous system: preview of the upcoming 5th edition. *memo - Magazine of European Medical Oncology*. doi:10.1007/s12254-021-00680-x

Sfeir, A., & de Lange, T. (2012). Removal of shelterin reveals the telomere end-protection problem. *Science, 336*(6081), 593-597. doi:10.1126/science.1218498

Sfeir, A., Kosiyatrakul, S. T., Hockemeyer, D., MacRae, S. L., Karlseder, J., Schildkraut, C. L., & de Lange, T. (2009). Mammalian telomeres resemble fragile sites and require TRF1 for efficient replication. *Cell, 138*(1), 90-103. doi:10.1016/j.cell.2009.06.021

Shah, A. H., Snelling, B., Bregy, A., Patel, P. R., Tememe, D., Bhatia, R., . . . Komotar, R. J. (2013). Discriminating radiation necrosis from tumor progression in gliomas: a systematic review what is the best imaging modality? *J Neurooncol, 112*(2), 141-152. doi:10.1007/s11060-013-1059-9

Shay, J. W., & Wright, W. E. (2019). Telomeres and telomerase: three decades of progress. *Nat Rev Genet, 20*(5), 299-309. doi:10.1038/s41576-019-0099-1

Simon, M., Hosen, I., Gousias, K., Rachakonda, S., Heidenreich, B., Gessi, M., . . . Kumar, R. (2015). TERT promoter mutations: a novel independent prognostic factor in primary glioblastomas. *Neuro Oncol, 17*(1), 45-52. doi:10.1093/neuonc/nou158

Simon, M., Hosen, I., Gousias, K., Rachakonda, S., Heidenreich, B., Gessi, M., . . . Kumar, R. (2015). TERT promoter mutations: a novel independent prognostic factor in primary glioblastomas. *Neuro-oncology, 17*(1), 45-52. doi:10.1093/neuonc/nou158

Stupp, R., Mason, W. P., van den Bent, M. J., Weller, M., Fisher, B., Taphoorn, M. J., . . . Mirimanoff, R. O. (2005). Radiotherapy plus concomitant and adjuvant temozolomide for glioblastoma. *N Engl J Med, 352*(10), 987-996. doi:10.1056/NEJMoa043330

Suchorska, B., Giese, A., Biczok, A., Unterrainer, M., Weller, M., Drexler, M., . . . Albert, N. L. (2018). Identification of time-to-peak on dynamic 18F-FET-PET as a prognostic marker specifically in IDH1/2 mutant diffuse astrocytoma. *Neuro Oncol, 20*(2), 279-288. doi:10.1093/neuonc/nox153

Suchorska, B., Jansen, N. L., Linn, J., Kretzschmar, H., Janssen, H., Eigenbrod, S., . . . Tonn, J. C. (2015). Biological tumor volume in 18FET-PET before radiochemotherapy correlates with survival in GBM. *Neurology, 84*(7), 710-719. doi:10.1212/wnl.0000000000001262

Surovtseva, Y. V., Churikov, D., Boltz, K. A., Song, X., Lamb, J. C., Warrington, R., . . . Shippen, D. E. (2009). Conserved telomere maintenance component 1 interacts with STN1 and maintains chromosome ends in higher eukaryotes. *Mol Cell, 36*(2), 207-218. doi:10.1016/j.molcel.2009.09.017

Tan, A. C., Ashley, D. M., López, G. Y., Malinzak, M., Friedman, H. S., & Khasraw, M. (2020). Management of glioblastoma: State of the art and future directions. *CA Cancer J Clin, 70*(4), 299-312. doi:10.3322/caac.21613

Taphoorn, M. J., Sizoo, E. M., & Bottomley, A. (2010). Review on quality of life issues in patients with primary brain tumors. *Oncologist, 15*(6), 618-626. doi:10.1634/theoncologist.2009-0291

Thon, N., Kunz, M., Lemke, L., Jansen, N. L., Eigenbrod, S., Kreth, S., . . . Kreth, F. W. (2015). Dynamic 18F-FET PET in suspected WHO grade II gliomas defines distinct biological subgroups with different clinical courses. *Int J Cancer, 136*(9), 2132-2145. doi:10.1002/ijc.29259

Tian, H., Wu, H., Wu, G., & Xu, G. (2020). Noninvasive Prediction of TERT Promoter Mutations in High-Grade Glioma by Radiomics Analysis Based on Multiparameter MRI. *Biomed Res Int, 2020*, 3872314. doi:10.1155/2020/3872314

Tian, Q., Yan, L. F., Zhang, X., Zhang, X., Hu, Y. C., Han, Y., . . . Cui, G. B. (2018). Radiomics strategy for glioma grading using texture features from multiparametric MRI. *J Magn Reson Imaging, 48*(6), 1518-1528. doi:10.1002/jmri.26010

van Griethuysen, J. J. M., Fedorov, A., Parmar, C., Hosny, A., Aucoin, N., Narayan, V., . . . Aerts, H. (2017). Computational Radiomics System to Decode the Radiographic Phenotype. *Cancer Res, 77*(21), e104-e107. doi:10.1158/0008-5472.Can-17-0339

Van Meir, E. G., Hadjipanayis, C. G., Norden, A. D., Shu, H. K., Wen, P. Y., & Olson, J. J. (2010). Exciting new advances in neuro-oncology: the avenue to a cure for malignant glioma. *CA Cancer J Clin, 60*(3), 166-193. doi:10.3322/caac.20069

van Velden, F. H., Kramer, G. M., Frings, V., Nissen, I. A., Mulder, E. R., de Langen, A. J., . . . Boellaard, R. (2016). Repeatability of Radiomic Features in Non-Small-Cell Lung Cancer [(18)F]FDG-PET/CT Studies: Impact of Reconstruction and Delineation. *Mol Imaging Biol, 18*(5), 788-795. doi:10.1007/s11307-016-0940-2

Vander Borght, T., Asenbaum, S., Bartenstein, P., Halldin, C., Kapucu, O., Van Laere, K., . . . Tatsch, K. (2006). EANM procedure guidelines for brain tumour imaging using labelled amino acid analogues. *Eur J Nucl Med Mol Imaging, 33*(11), 1374-1380. doi:10.1007/s00259-006-0206-3

Vettermann, F., Suchorska, B., Unterrainer, M., Nelwan, D., Forbrig, R., Ruf, V., . . . Albert, N. L. (2019). Non-invasive prediction of IDH-wildtype genotype in gliomas using dynamic 18F-FET PET. *European Journal of Nuclear Medicine and Molecular Imaging, 46*(12), 2581-2589. doi:10.1007/s00259-019-04477-3

Vinagre, J., Almeida, A., Pópulo, H., Batista, R., Lyra, J., Pinto, V., . . . Soares, P. (2013). Frequency of TERT promoter mutations in human cancers. *Nat Commun, 4*, 2185. doi:10.1038/ncomms3185

Vredenburgh, J. J., Desjardins, A., Herndon, J. E., 2nd, Marcello, J., Reardon, D. A., Quinn, J. A., . . . Friedman, H. S. (2007). Bevacizumab plus irinotecan in recurrent glioblastoma

multiforme. *J Clin Oncol, 25*(30), 4722-4729. doi:10.1200/jco.2007.12.2440

Wang, B., Zhang, S., Wu, X., Li, Y., Yan, Y., Liu, L., . . . Yan, T. (2021). Multiple Survival Outcome Prediction of Glioblastoma Patients Based on Multiparametric MRI. *Front Oncol, 11*, 778627. doi:10.3389/fonc.2021.778627

Wang, S., Xiao, F., Sun, W., Yang, C., Ma, C., Huang, Y., . . . Xu, H. (2021). Radiomics Analysis Based on Magnetic Resonance Imaging for Preoperative Overall Survival Prediction in Isocitrate Dehydrogenase Wild-Type Glioblastoma. *Front Neurosci, 15*, 791776. doi:10.3389/fnins.2021.791776

Weckesser, M., Langen, K. J., Rickert, C. H., Kloska, S., Straeter, R., Hamacher, K., . . . Schober, O. (2005). O-(2-[18F]fluorethyl)-L-tyrosine PET in the clinical evaluation of primary brain tumours. *Eur J Nucl Med Mol Imaging, 32*(4), 422-429. doi:10.1007/s00259-004-1705-8

Wen, P. Y., & Kesari, S. (2008). Malignant gliomas in adults. *N Engl J Med, 359*(5), 492-507. doi:10.1056/NEJMra0708126

Werner, J. M., Stoffels, G., Lichtenstein, T., Borggrefe, J., Lohmann, P., Ceccon, G., . . . Galldiks, N. (2019). Differentiation of treatment-related changes from tumour progression: a direct comparison between dynamic FET PET and ADC values obtained from DWI MRI. *Eur J Nucl Med Mol Imaging, 46*(9), 1889-1901. doi:10.1007/s00259-019-04384-7

Wester, H. J., Herz, M., Weber, W., Heiss, P., Senekowitsch-Schmidtke, R., Schwaiger, M., & Stöcklin, G. (1999). Synthesis and radiopharmacology of O-(2-[18F]fluoroethyl)-L-tyrosine for tumor imaging. *J Nucl Med, 40*(1), 205-212.

Xi, Y. B., Guo, F., Xu, Z. L., Li, C., Wei, W., Tian, P., . . . Yin, H. (2018). Radiomics signature: A potential biomarker for the prediction of MGMT promoter methylation in glioblastoma. *J Magn Reson Imaging, 47*(5), 1380-1387. doi:10.1002/jmri.25860

Xu, J., Ren, Y., Zhao, X., Wang, X., Yu, X., Yao, Z., . . . Wang, H. (2022). Incorporating multiple magnetic resonance diffusion models to differentiate low- and high-grade adult gliomas: a machine learning approach. *Quant Imaging Med Surg, 12*(11), 5171-5183. doi:10.21037/qims-22-145

Yan, J., Chu-Shern, J. L., Loi, H. Y., Khor, L. K., Sinha, A. K., Quek, S. T., . . . Townsend, D. (2015). Impact of Image Reconstruction Settings on Texture Features in 18F-FDG PET. *J Nucl Med, 56*(11), 1667-1673. doi:10.2967/jnumed.115.156927

Young, R. J., Gupta, A., Shah, A. D., Graber, J. J., Zhang, Z., Shi, W., . . . Omuro, A. M. (2011). Potential utility of conventional MRI signs in diagnosing pseudoprogression in glioblastoma. *Neurology, 76*(22), 1918-1924. doi:10.1212/WNL.0b013e31821d74e7

Zwanenburg, A., Vallières, M., Abdalah, M. A., Aerts, H., Andrearczyk, V., Apte, A., . . . Löck, S. (2020). The Image Biomarker Standardization Initiative: Standardized Quantitative Radiomics for High-Throughput Image-based Phenotyping. *Radiology, 295*(2), 328-338. doi:10.1148/radiol.2020191145

Acknowledgements